Experimental Evaluation of Semiactive Magneto-Rheological Suspensions for Passenger Vehicles

by

Christopher A. Paré

Thesis submitted to the Faculty of the

Virginia Polytechnic Institute and State University

in partial fulfillment of the requirements for the degree of

Master of Science

in

Mechanical Engineering

Mehdi Ahmadian, Chair
Douglas J. Nelson
William R. Saunders

May 1998
Blacksburg, Virginia

Keywords: Semiactive, Magneto-Rheological, Skyhook, Groundhook, Damper, Experimental, Vehicle Dynamics

EXPERIMENTAL EVALUATION OF SEMIACTIVE MAGNETO-RHEOLOGICAL SUSPENSIONS FOR PASSENGER VEHICLES

by

Christopher A. Paré

Mehdi Ahmadian, Chairman

Mechanical Engineering

This study experimentally evaluates the dynamic response of a single vehicle suspension incorporating a magneto-rheological (MR) damper. A full-scale two-degree-of-freedom (2DOF) quarter-car test apparatus has been constructed at the Advanced Vehicle Dynamics Lab at Virginia Tech to evaluate the response of a vehicle suspension under the different control schemes of skyhook, groundhook, and hybrid semiactive control. The quarter-car apparatus was constructed using materials from 80/20 Incorporated and a hydraulic actuation system from MTS. A dSPACE AutoBox was used both for controlling the MR dampers and acquiring data.

The first task was to understand the baseline dynamic response of the quarter-car system with only a passive damper. Next, the passive damper was replaced with a controllable MR damper. The control schemes of skyhook, groundhook, and hybrid semiactive control were applied to the MR damper. The physical response of the quarter-car with the different control schemes was then compared to the analytical prediction for the response, with favorable results. The response of the quarter-car with the semiactive damper was also compared to the response of the quarter-car with a passive damper, and the resulting limitations of passive damping are discussed.

Finally, the practical implications of this study are shown in a discussion of the physical implementation of the MR dampers in the Virginia Tech FutureCar, a full-size Chevrolet Lumina. Although the actual skyhook, groundhook, and hybrid semiactive control schemes were not implemented on the vehicle, the results were promising and generated several recommendations for future research.

Acknowledgments

I would like to thank my advisor, Dr. Mehdi Ahmadian, for his help and encouragement throughout graduate studies in the Mechanical Engineering Department. I would also like to thank Drs. Douglas Nelson and William Saunders for serving on my graduate committee. I also would like to thank Lord Corporation and Koni Incorporated for donating the time and technical expertise to supply the Advanced Vehicle Dynamics Lab at Virginia Tech with the hardware used for this study. The generous donations by PCB Piezotronics Incorporated, Texas Instruments Incorporated, and the 80/20 Corporation, which made possible the many tests that were required for this study, are greatly appreciated.

Finally I would like to thank my wife, Sarah, my mother and stepfather, Carol Paré and Robert Beaudette, my sister, Kim, and G for all their love and support during the time I have spent at Virginia Tech.

Contents

List of Figures

List of Tables

Chapter 1

Introduction

The purpose of this chapter is to provide the reader with an introduction to the research conducted for this thesis. First, the shortcomings of conventional passive vehicle suspensions will be discussed. Several known methods for using electronically controlled suspensions to overcome the limitations of passive suspensions will then be presented. The results of a literature search conducted in the areas related to this research will then be discussed. The chapter ends with the objectives for the research conducted, followed by an outline of the subsequent chapters of this work.

1.1 The Classic Vehicle Suspension Compromise

Traditionally, automotive suspension designs have been a compromise between the two conflicting criteria of road holding and passenger comfort. The suspension system must support the weight of the vehicle, provide directional control during handling maneuvers, and provide effective isolation of passengers and payload from road disturbances [1].

A passive suspension has the ability to store energy via a spring and to dissipate it via a damper. The parameters are generally fixed, being chosen to achieve a certain level of compromise between road holding and ride comfort. Once the spring has been selected based on the load-carrying capability of the suspension, the damper is the only variable remaining to specify. Low damping yields poor resonance control at the natural frequencies of the body (sprung mass) and axle (unsprung mass), but provides the necessary high frequency isolation required for a comfortable ride. Conversely, large damping results in good resonance control at the expense of high frequency isolation.

Due to these conflicting demands, suspension design has had to be something of a compromise, largely determined by the type of use for which the vehicle is designed.

Electronically controlled suspension systems are considered to be a way of increasing the freedom one has to specify independently the characteristics of handling and ride quality. Skyhook control has been shown to be an effective means of nearly eliminating the compromise between resonance control and high frequency isolation [2]. Groundhook control has been shown to be an effective means of controlling the dynamic axle loading which results in excessive tire forces and pavement damage [3]. In this capacity, groundhook control has found acceptance in the area of heavy truck vehicle dynamics. More recently, a control scheme has been developed which utilizes a linear combination of skyhook and groundhook control. With this hybrid control scheme, the suspension can be tuned to respond exactly as it would with skyhook control or groundhook control. In addition, the suspension can be adjusted such that it responds as a combination of the two, with more or less influence given to the skyhook or groundhook component [4].

1.2 Methods of Suspension Control

The key element in any of the aforementioned control schemes is some form of force generator. Fully active force generators are capable of providing an arbitrary force to the vehicle suspension in either direction, jounce or rebound. The physical implementation of a fully active force generator is usually a hydraulic actuator and power supply. It has been shown that fully active suspensions require a considerable amount of energy to actuate and can be quite complex [5].

Another type of force generator is classified as a semiactive force generator, or semiactive damper. A semiactive damper generates force in a passive manner, but the amount of force generated is actively controlled. The damping control is typically accomplished with an adjustable orifice or, as in this study, with a fixed orifice and a fluid with adjustable viscosity, such as a magneto-rheological (MR) fluid.

1.3 Literature Review

A literature search was conducted to investigate the past research done in any of the areas relating to this work. The areas of semiactive control, magneto-rheological dampers, and quarter-car testing are of primary interest. Fig. 1.1 displays a flowchart of the literature search according to the keywords used. Two databases, INSPEC and Compendex, were used for the literature search. INSPEC is a database for physics, electronics, and computing, while Compendex is the Comprehensive Engineering Index.

As expected, the union of any two of the primary keywords resulted in a more manageable number of hits. As such, all works that were reviewed were taken from the second tier of the flowchart to avoid searching through large numbers of possibly unrelated papers. In addition to the papers reviewed, many books and other papers related to the areas of vehicle dynamics, semiactive suspension control, and magneto-rheological dampers have been read and consulted over the course of this project.

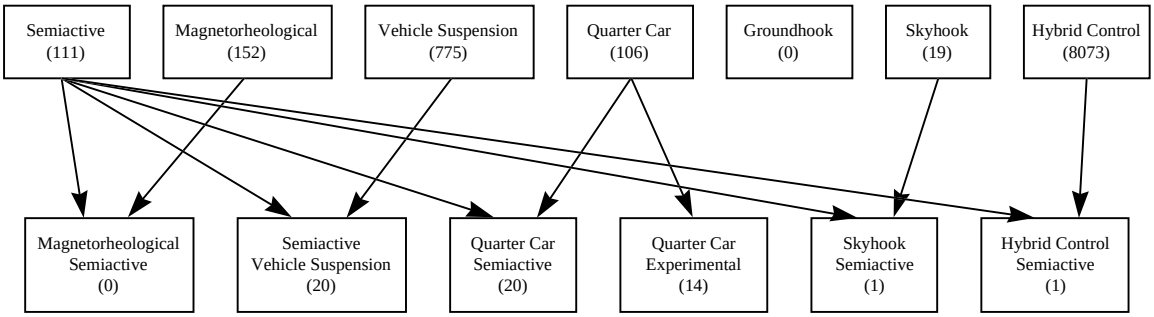

Figure 1.1. Literature Search Flowchart

1.3.1 Keyword: Semiactive

Research in the area of semiactive suspensions has been conducted since the early seventies. Most studies in the area of semiactive suspensions used a two-degree-of-freedom model representing single suspensions. Lieh [6] explores the use of semiactive suspensions to control the dynamics of a full car model. He concludes that the skyhook

control policy reduces the RMS acceleration of the car body while increasing the RMS tire forces.

The study by Margolis [7] examines the effects of using realistic feedback signals when controlling active and semiactive suspension systems. This is an analytical study that suggests several feedback strategies for the semiactive suspension system so that the performance can approach the fully active suspension performance. In another study by Margolis [8], he outlines a procedure to examine the feasibility of using semiactive or active vibration isolation instead of purely passive approaches.

Hwang *et al.* [9] present an interesting method for testing the semiactive damper hardware without using a complete vehicle. They explore the test method known as a hardware-in-the-loop simulation. Essentially, the dynamic model of the system is coded for simulation in a computer. The piece of hardware under test (i.e., the semiactive damper) is excited according to the computer numerical simulation, and the response of the hardware is measured and fed back into the computer to complete the simulation.

Miller [10] explored the effects of the levels of both on-state and off-state damping on the performance of the quarter-car semiactive suspension system. The continuous semiactive suspension is also considered. Bellizzi and Bouc [11] and Hrovat *et al*. [12] studied optimal control techniques for the semiactive suspension.

1.3.2 Keyword: Magneto-rheological

The first three studies cited in the area of magneto-rheological fluids deal with characterizing the properties of MR fluids. Lazareva and Shitik [13] studied the properties of MR fluids that are based on barium and strontium ferrites and iron oxides. The fluids were prepared using various combinations of the materials, and their properties, such as the MR effect, were studied. Ashour *et al.* [14] studied the effects of components of the MR fluid on sedimentation of the magnetic particles and initial viscosity. An attempt was made to optimize the composition of the fluid such that the fluid had the desired properties. In another study, Ashour *et al.* [15] studied the general

composition of MR fluid along with the methods that are used to evaluate the performance of the fluids. There is also an introduction to the fundamental MR devices that exploit the MR effect.

The next three studies cited explore the design of MR fluid devices. Carlson *et al.* [16] studied the advantages of MR over ER (electro-rheological) fluid devices in areas such as the yield strength, the required working volume of fluid, and the required power. The operational modes of the MR fluid are presented along with the linear fluid damper, the rotary brake, and the vibration damper. Kordonsky [17] developed the concept of the MR converter (or valve) and applies the MR converter to create devices such as the MR linear damper, the MR actuator, and the MR seal. Finally, Bolter and Janocha [18] examined the rules that should be applied when designing the magnetic circuit for MR devices that are working in the different modes of the MR fluid. Bolter and Janocha also examined the use of permanent magnets in the design of the magnetic circuit to change the operational point of the MR device.

The final magneto-rheological article by Jolly *et al*. [19] presents a model based on dipolar interaction of particles, and is used to predict the behavior of both MR fluids and MR elastomers. The model is compared to experimental data and it is shown that the model is semi-empirical in that it must be fit to the experimental data by adjusting a parameter that accounts for unmodeled magnetic interactions.

1.3.3 Keyword: Quarter-Car

The articles discovered in this category deal almost exclusively with theoretical quarter-car modeling of a vehicle suspension and the resulting numerical simulations. Lane *et al.* [20], however, experimentally test semiactive suspension systems on a scale model quarter-car assembly using an electromagnetic friction clutch as a semiactive force generator. The quarter-car apparatus used was a scaled-down model with lower masses and stiffnesses, but with the same modal frequencies as a full-scale quarter-car.

1.3.4 Keyword: Skyhook

Of the nineteen articles hit using the keyword "skyhook," only four were found to be of relevance. Karnopp [21] contributes an excellent review of many of the past efforts in the area of semiactive suspension design. He also presents a background of the information that is required to understand semiactive suspension systems. Finally, he discusses several semiactive suspension applications.

Cebon *et al.* [22] discuss the different control strategies that are available for 2DOF semiactive systems. They apply semiactive control and linear optimal control with full-state feedback along with simple on-off control strategies in order to reduce both the tire force and body acceleration of a heavy truck. They compare the results of their mathematical simulations to their experimental testing using a hardware-in-the-loop test method. They conclude that, compared to passive suspensions, the full state feedback methods work the best in reducing tire loads and body acceleration according to simulation and experimental results.

Finally, the skyhook study by Satoh *et al*. [23] is a practical realization of a fully active skyhook suspension system on a passenger vehicle. The controller responds to the pitch and roll motions of the vehicle, as well as to the vertical motion of the wheels. The results in an actual vehicle showed marked improvement over the passive suspension.

1.4 Research Objective

The primary objective of this study is the application of magneto-rheological dampers to vehicle primary suspensions. Specifically, the experimental results of hybrid semiactive control will be compared to the results of passive, skyhook, and groundhook control in terms of the single suspension (quarter-car) dynamic response.

1.5 Outline

Chapter 2 presents the background information necessary to understand skyhook, groundhook, and hybrid semiactive control of suspension systems. It also provides an introduction to the design, construction, and performance of a magneto-rheological damper. Chapter 3 describes, in detail, the test structure used to evaluate the dynamic response of the single suspension. The structural design considerations of the quarter-car apparatus are discussed, along with the actuation system used to excite the quarter-car, and the data acquisition system used to analyze the dynamic response of the system. This chapter also presents the experimental setup of the quarter-car apparatus pertaining to the semiactive MR damper control. This chapter discusses the excitation signals used for the quarter-car, as well as the sensory information supplied to the dSPACE controller. Chapter 4 discusses the results of all the laboratory testing involving the quarter-car apparatus. Chapter 5 highlights the practical implications of MR dampers with a discussion of the physical implementation of the Lord/Koni MR dampers in a midsize family sedan. Finally, Chapter 6 summarizes the results of this study and provides recommendations for future work.

Chapter 2

Background

The purpose of this chapter is to provide the background for the research conducted in this study. First, three different theoretical control schemes for a two-degree-of-freedom (2DOF) system will be presented. In addition to the individual algorithms, the aim of each control scheme will be shown with the intended performance benefits. The discussion will then turn to the physical implementation of these control schemes on a 2DOF system. The chapter will conclude with a discussion of the practical design considerations and performance of a semiactive MR damper.

2.1 2DOF Passive Suspension System

A typical vehicle primary suspension can be modeled as shown in Fig. 2.1. Since the model represents a single suspension from one of the four corners of the vehicle, this 2DOF system is often referred to as the "quarter-car" model.

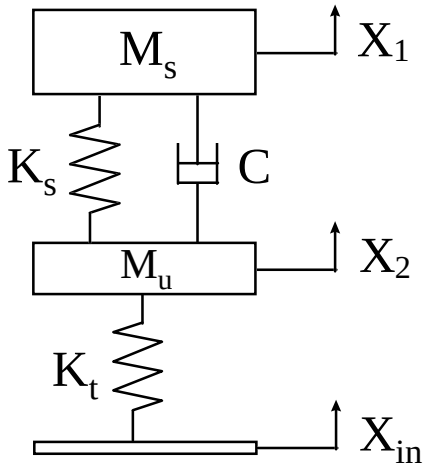

Figure 2.1. 2DOF "Quarter-Car Model"

The input to this model is a displacement input which is representative of a typical road profile. The input excites the first degree of freedom (the unsprung mass of a quarter of the vehicle, representing the wheel, tire, and some suspension components) through a spring element which represents the tire stiffness. The unsprung mass is connected to the second degree of freedom (the sprung mass, representing the body of the vehicle) through the primary suspension spring and damper. The transmissibility of the 2DOF system, if all the elements of the quarter-car are passive, is shown in Fig. 2.2 for various damping coefficients. The first plot shows the displacement of the sprung mass (X_1) with respect to the input (X_{in}), while the second plot shows the displacement of the unsprung mass (X_2) with respect to the input (X_{in}).

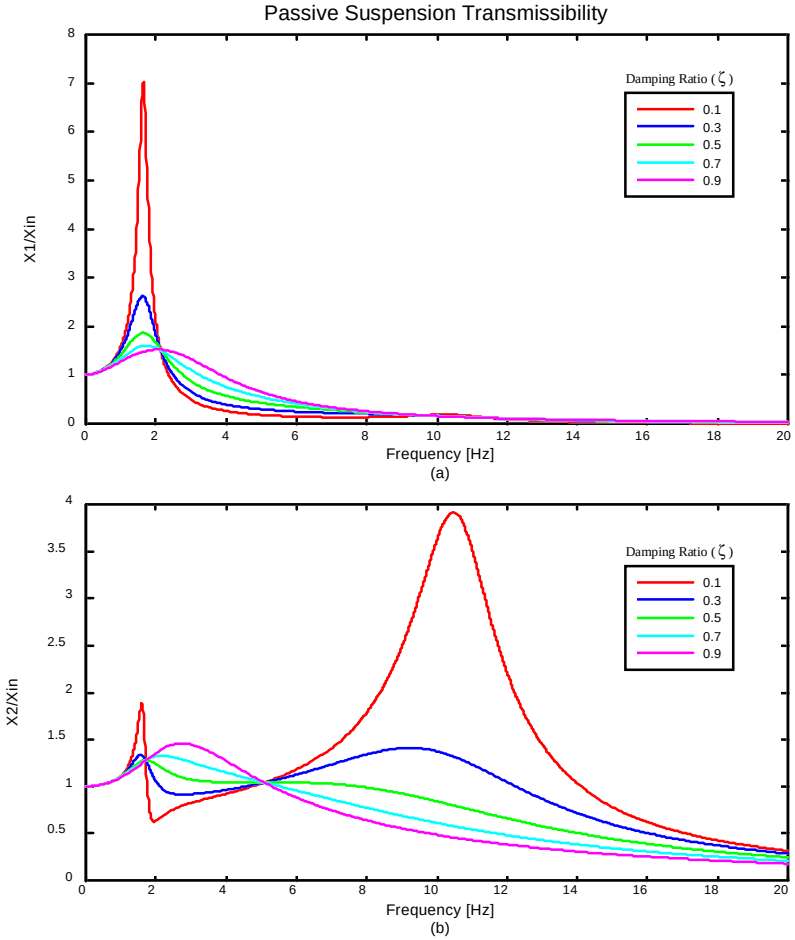

Figure 2.2. Passive Suspension Transmissibility
(a) Sprung Mass Transmissibility (b) Unsprung Mass Transmissibility

Notice that at low passive damping, the resonant transmissibility (around $\omega = \omega_{n1}$ or 1.7 Hz and $\omega = \omega_{n2}$ or 10.5Hz) is relatively large, while the transmissibility at higher frequencies is quite low. As the damping is increased, the resonant peaks are attenuated, but isolation is lost both at high frequency and at frequencies between the two natural frequencies of the system. The lack of isolation between the two natural frequencies is caused by the increased coupling of the two degrees of freedom with a stiffer damper. The lack of isolation at higher frequencies will result in a harsher vehicle ride. These transmissibility plots graphically illustrate the inherent tradeoff between resonance control and high frequency isolation that is associated with the design of passive vehicle suspension systems.

The parameters used in the simulation of this model are the actual system parameters of the physical quarter-car apparatus described in Chapter 3. These system parameters, which closely model actual vehicle parameters, are shown in Table 2.1.

Table 2.1. System Parameters Used in Quarter-Car Model

Parameter	**Value**
Sprung Mass (M_s)	310 kg
Unsprung Mass (M_u)	45 kg
Suspension Stiffness (K_s)	40,000 N/m
Tire Stiffness (K_t)	190,000 N/m

The equations of motion for the 2DOF system can be written in matrix form as

$$\begin{bmatrix} m_s & 0 \\ 0 & m_u \end{bmatrix} \begin{Bmatrix} \ddot{x}_1 \\ \ddot{x}_2 \end{Bmatrix} + \begin{bmatrix} c & -c \\ -c & c \end{bmatrix} \begin{Bmatrix} \dot{x}_1 \\ \dot{x}_2 \end{Bmatrix} + \begin{bmatrix} k_s & -k_s \\ -k_s & k_s + k_t \end{bmatrix} \begin{Bmatrix} x_1 \\ x_2 \end{Bmatrix} = \begin{bmatrix} 0 \\ k_t \end{bmatrix} x_{in} \qquad (2.1)$$

Knowing the physical parameters of the 2DOF system, we can calculate the damping ratio for each DOF. To facilitate this calculation, we will treat the system as two 1DOF systems. In order to present the transmissibility plots as a function of damping ratio

rather than damping coefficient, we can decouple the equations of motion by neglecting the off-diagonal terms, and then calculate the damping ratio as

$$\varsigma_1 = \frac{c}{2\sqrt{k_s m_s}} \tag{2.2}$$

$$\varsigma_2 = \frac{c}{2\sqrt{(k_s + k_t) m_u}} \tag{2.3}$$

While this method of calculating the damping ratio is only valid at low damping, the intent is not to precisely define the damping ratio, but rather to show the effects of increased damping on transmissibility.

2.2 Control Schemes for a 2DOF System

This section will introduce the three 2DOF control schemes of interest in this study. Skyhook, groundhook, and hybrid semiactive control will be presented and compared with a typical 2DOF passive suspension.

2.2.1 Skyhook Control

The skyhook damper configuration attempts to eliminate the tradeoff between resonance control and high frequency isolation common to passive suspensions [24]. Consider the arrangement in Fig. 2.3. The damper is connected to an inertial reference in the sky. Clearly, this arrangement is fictitious, since for this configuration to be implemented, the damper would have to be connected to a reference point which is fixed with respect to the ground but can translate with the vehicle. Such a suspension mounting point does not exist. The end goal of skyhook control is not to physically implement this system, but to command a controllable damper to cause the system to respond in a similar manner to this fictitious system.

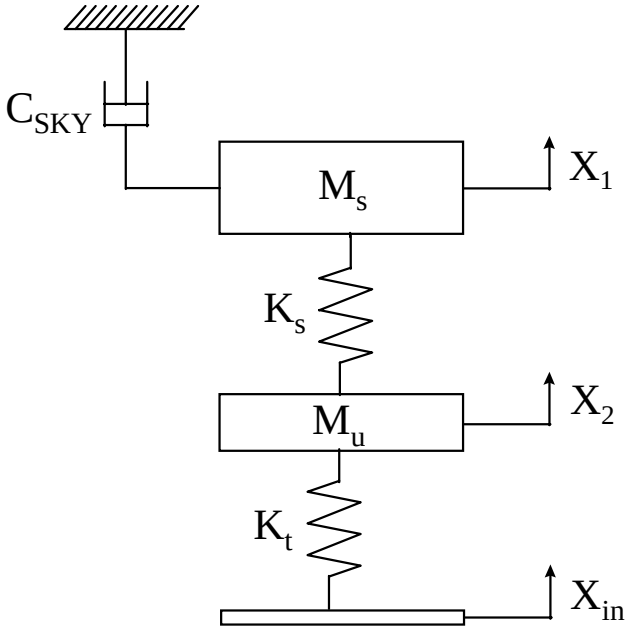

Figure 2.3. Skyhook Damper Configuration

The transmissibility for this system is shown in Fig. 2.4 for different values of the skyhook damping coefficient, C_{sky}. Notice that as the skyhook damping ratio increases, the resonant transmissibility near ω_{n1} decreases, even to the point of isolation, but the transmissibility near ω_{n2} increases. In essence, this skyhook configuration is adding more damping to the sprung mass and taking away damping from the unsprung mass. The skyhook configuration is ideal if the primary goal is isolating the sprung mass from base excitations [21], even at the expense of excessive unsprung mass motion. An additional benefit is apparent in the frequency range between the two natural frequencies. With the skyhook configuration, isolation in this region actually increases with increasing C_{sky}.

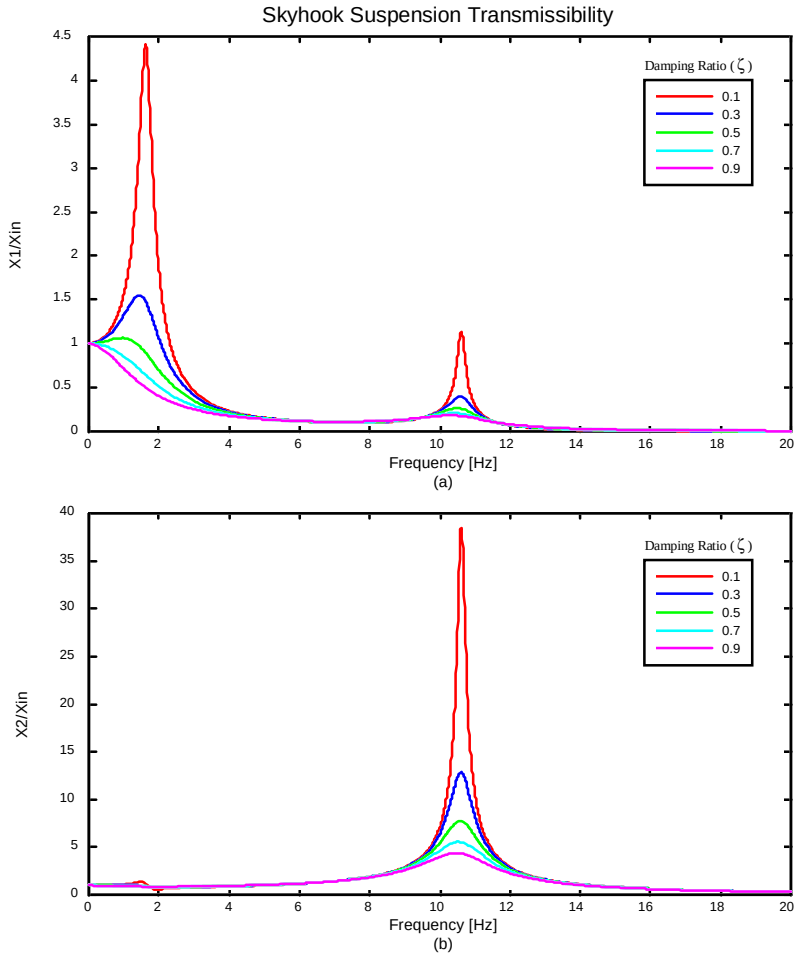

Figure 2.4. Skyhook Configuration Transmissibility
(a) Sprung Mass Transmissibility (b) Unsprung Mass Transmissibility

As stated earlier, the skyhook configuration, while beneficial from an analysis standpoint, is impossible to physically implement. Several methods exist for generating the equivalent skyhook damping force without actually attaching a damper to an inertial reference point. One method is to remove the passive suspension (i.e., both the damper and the spring) and replace it with an active force generator. A fully active force generator can be realized by using a hydraulic actuator, however, the resulting system is rather complex and requires a significant amount of power [24]. Another approach to achieving skyhook damping is to use semiactive dampers. Semiactive dampers allow for the damping coefficient, and therefore the damping force, to be varied between high and

low levels of damping. Early semiactive dampers were mechanically adjustable by opening or closing a bypass valve. The only power required for the damper is the relatively small power to actuate the valve. For this research, a magneto-rheological damper which varies the damping by electrically changing the magnetic field applied to the magneto-rheological fluid is used. With a semiactive damper, the 2DOF model shown in Fig. 2.1 modifies to Fig. 2.5, where the damping coefficient, $C_{controllable}$, can be varied in time. This configuration will be referred to as a semiactive suspension.

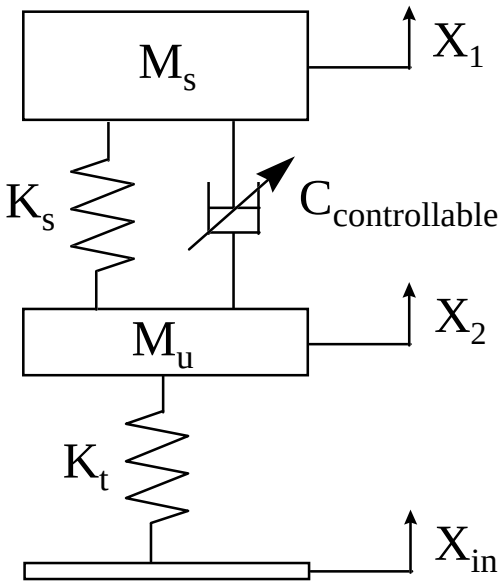

Figure 2.5. Semiactive Suspension

Once it is decided that a semiactive damper will be used, the means of modulating the damper such that it emulates a skyhook damper must be determined. We first define the velocity of the sprung mass relative to the unsprung mass, V_{12}, to be positive when the sprung mass and unsprung mass are separating (i.e., when V_1 is greater than V_2) for the systems shown in Figures 2.3 and 2.5. Now assume that for both systems, the sprung mass is moving upwards with a positive velocity V_1. If we consider the force that is applied by the skyhook damper to the sprung mass, we notice that it is in the negative X_1 direction, or

$$F_{SKY} = -C_{SKY} V_1 \tag{2.4}$$

where F_{SKY} is the skyhook force. Next, we need to determine if the semiactive damper is able to provide the same force. If the sprung and unsprung masses in Fig. 2.5 are separating, then the semiactive damper is in tension. Thus, the force applied to the sprung mass is in the negative X_1 direction, or

$$F_{CONTROLLABLE} = -C_{CONTROLLABLE} V_{12} \tag{2.5}$$

where $F_{CONTROLLABLE}$ is the force applied to the sprung mass. Since we are able to generate a force in the proper direction, the only requirement to match the skyhook suspension is

$$C_{CONTROLLABLE} = C_{SKY} \frac{V_1}{V_{12}} \tag{2.6}$$

To summarize, if V_1 and V_{12} are positive, $C_{CONTROLLABLE}$ should be defined as in Eq. (2.6).

Now consider the case in which the sprung and unsprung masses are still separating, but the sprung mass is moving downwards with a negative velocity V_1. In the skyhook configuration, the damping force will now be applied in the upwards, or positive, X_1 direction. In the semiactive configuration, however, the semiactive damper is still in tension, and the damping force will still be applied in the downwards, or negative, direction. Since the semiactive damping force cannot possibly be applied in the same direction as the skyhook damping force, the best that can be achieved is to minimize the damping force. Ideally, the semiactive damper is desired to be set so that there is no damping force, but in reality there is some small damping force present and it is not in the same direction as the skyhook damping force. Thus, if V_{12} is positive and V_1 is negative, we need to minimize the semiactive damping force.

We can apply the same simple analysis to the other two combinations of V_1 and V_{12}, resulting in the well-known semiactive skyhook control policy [25]:

$$\begin{cases} V_1 V_{12} > 0 & F_{SA} = C_{SKY} V_1 \\ V_1 V_{12} < 0 & F_{SA} = 0 \end{cases} \tag{2.7}$$

where F_{SA} is the semiactive skyhook damper force. Equation (2.7) implies that when the relative velocity across the suspension (V_{12}) and the sprung mass absolute velocity (V_1) have the same sign, a damping force proportional to V_1 is desired. Otherwise, the minimal amount of damping is desired. Further, Eq. (2.7) provides a very simple method to emulate the ideal skyhook suspension system using only a semiactive damper.

2.2.2 Groundhook Control

Consider modifying the skyhook damper configuration so that the damper is connected to M_u (the unsprung mass) rather than M_s (the sprung mass). The resulting system is referred to as the groundhook damper configuration, and is shown in Fig 2.6.

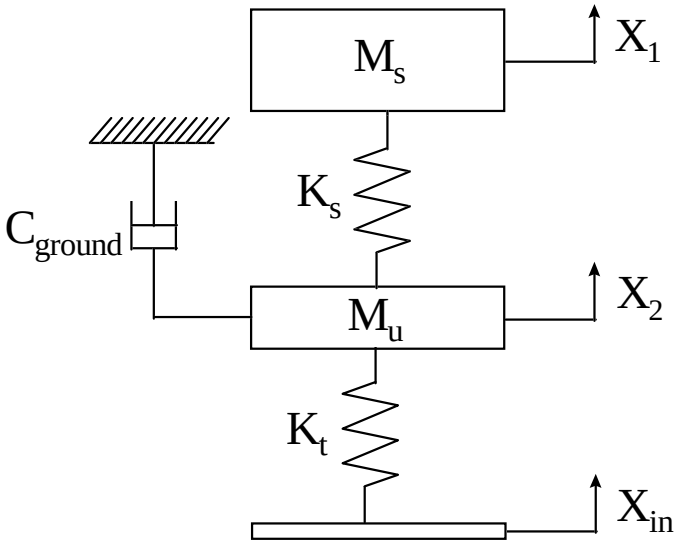

Figure 2.6. Groundhook Damper Configuration

The system response of the groundhook configuration is similar to the response of the skyhook configuration, with the obvious difference that the groundhook configuration effectively adds damping to the unsprung mass and removes it from the sprung mass. As seen in the transmissibility plots of Fig. 2.7, the groundhook configuration excels at

isolating the unsprung mass from the input excitation, this time at the expense of sprung mass motion.

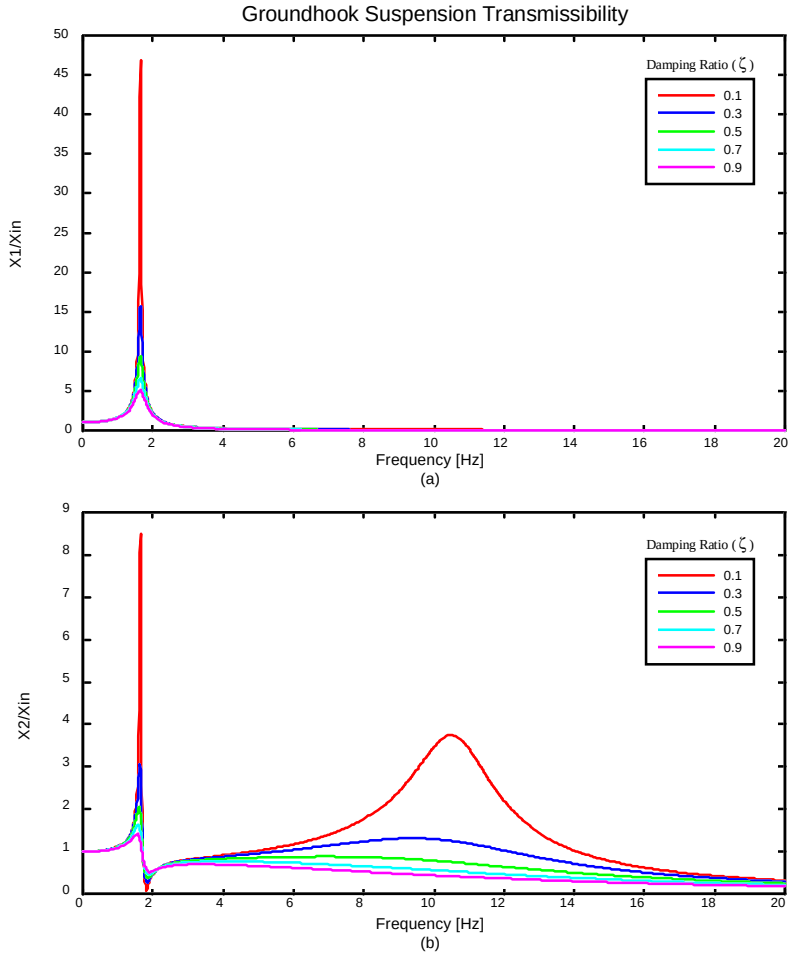

Figure 2.7. Groundhook Configuration Transmissibility
(a) Sprung Mass Transmissibility (b) Unsprung Mass Transmissibility

If the same reasoning used for the skyhook configuration above is used for the groundhook configuration, it can easily be shown that the groundhook semiactive control policy reduces to

$$\begin{cases} -V_2 V_{12} > 0 & F_{SA} = C_{GND} V_2 \\ -V_2 V_{12} < 0 & F_{SA} = 0 \end{cases} \tag{2.8}$$

2.2.3 Hybrid Control

An alternative semiactive control policy known as hybrid control has been shown to take advantage of the benefits of both skyhook and groundhook control [4]. With hybrid control, the user has the ability to specify how closely the controller emulates skyhook or groundhook. In other words, hybrid control can divert the damping energy to the bodies in a manner that eliminates the compromise that is inherent in passive dampers. The hybrid configuration is shown in Fig. 2.8.

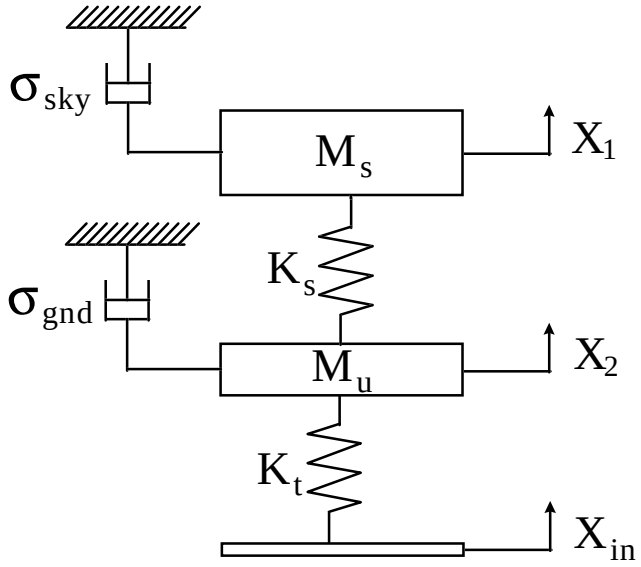

Figure 2.8. Hybrid Configuration

The hybrid control policy is a linear combination of Eqs. (2.7) and (2.8) and can be written as

$$\left\{\begin{matrix} V_1 V_{12} > 0 & \sigma_{SKY} = V_1 \\ V_1 V_{12} < 0 & \sigma_{SKY} = 0 \end{matrix}\right\}$$

$$\left\{F_{SA} = G\left[\alpha\sigma_{SKY} + (1-\alpha)\sigma_{GND}\right]\right. \tag{2.9}$$

$$\left\{\begin{matrix} -V_2 V_{12} > 0 & \sigma_{GND} = V_2 \\ -V_2 V_{12} < 0 & \sigma_{GND} = 0 \end{matrix}\right\}$$

where σ_{SKY} and σ_{GND} are the skyhook and groundhook components of the damping force. The variable α is the relative ratio between the skyhook and groundhook control, and G is

a constant gain. As the transmissibility plots in Fig. 2.9 show, when α is 1, the control policy reduces to pure skyhook, whereas when α is 0, the control is purely groundhook.

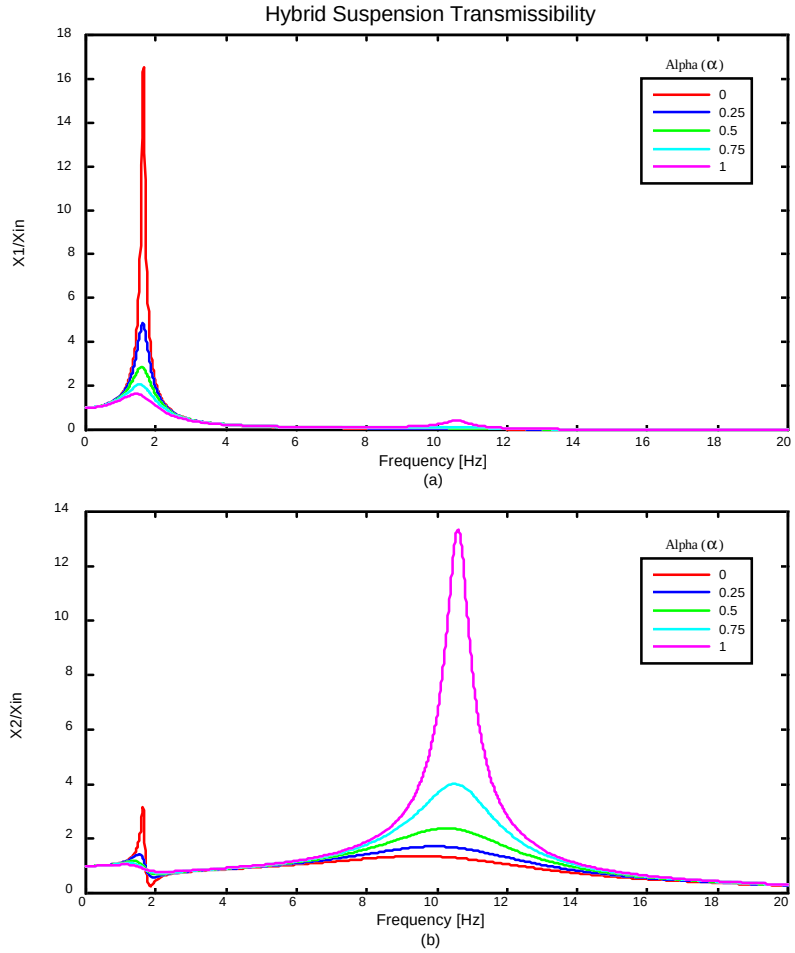

Figure 2.9. Hybrid Configuration Transmissibility
(a) Sprung Mass Transmissibility (b) Unsprung Mass Transmissibility

2.2.4 Comparison Between Passive and Semiactive Dampers

The previously mentioned benefits of semiactive dampers over passive dampers are clearly evident if we compare the transmissibilities for passive, skyhook, groundhook, and hybrid damping. Figure 2.10 shows the transmissibility of each at a damping ratio of 0.3.

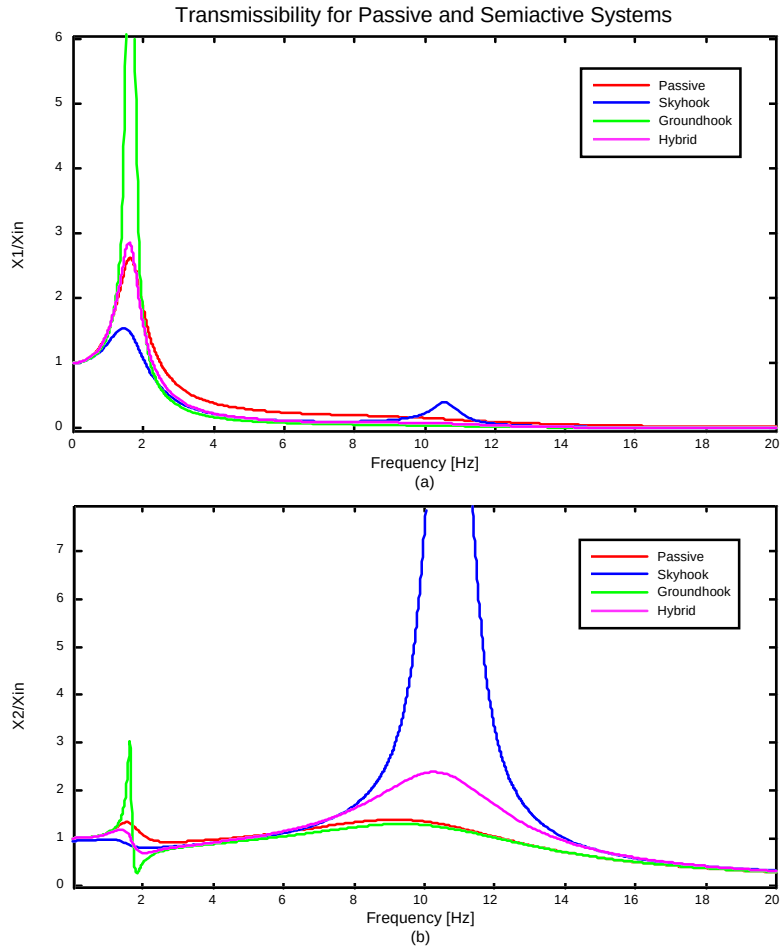

Figure 2.10. Transmissibility Comparison of Passive and Semiactive Dampers
(a) Sprung Mass Transmissibility (b) Unsprung Mass Transmissibility

2.3 Magneto-Rheological Dampers

The purpose of this section is to introduce the theoretical and practical applications of magneto-rheological (MR) fluid for a controllable MR damper. First, the concept of MR fluid will be introduced. Next, the practical realization of an MR damper will be discussed. Finally, the performance of the MR damper used for this research will be investigated.

2.3.1 Magneto-Rheological Fluids

Magneto-rheological fluids are materials that exhibit a change in rheological properties (elasticity, plasticity, or viscosity) with the application of a magnetic field. The MR effects are often greatest when the applied magnetic field is normal to the flow of the MR fluid. Another class of fluids that exhibit a rheological change is electro-rheological (ER) fluids. As the name suggests, ER fluids exhibit rheological changes when an electric field is applied to the fluid. However, there are many drawbacks to ER fluids, including relatively small rheological changes and extreme property changes with temperature. Although power requirements are approximately the same [16], MR fluids require only small voltages and currents, while ER fluids require very large voltages and very small currents. For these reasons, MR fluids have recently become a widely studied 'smart' fluid.

Besides the rheological changes that MR fluids experience while under the influence of a magnetic field, there are often other effects such as thermal, electrical, and acoustic property changes. However, in the area of vibration control, the MR effect is most interesting since it is possible to apply the effect to a hydraulic damper. The MR fluid essentially allows one to control the damping force of the damper by replacing mechanical valves commonly used in adjustable dampers. This offers the potential for a superior damper with little concern about reliability since if the MR damper ceases to be controllable, it simply reverts to a passive damper.

2.3.2 Construction of an MR Damper

Magneto-rheological fluids are manufactured by suspending ferromagnetic particles in a carrier fluid. The ferromagnetic particles are often carbonyl particles, since they are relatively inexpensive. Other particles, such as iron-cobalt or iron-nickel alloys, have been used to achieve higher yield stresses from the fluid [15]. Fluids containing these alloys are impractical for most applications due to the high cost of the cobalt or nickel alloys.

A wide range of carrier fluids such as silicone oil, kerosene, and synthetic oil can be used for MR fluids. The carrier fluid must be chosen carefully to accommodate the high temperatures to which the fluid can be subjected. The carrier fluid must be compatible with the specific application without suffering irreversible and unwanted property changes. The MR fluid must also contain additives to prevent the sedimentation of, and promote the dispersion of, the ferromagnetic particles.

A functional representation of an MR damper, with schematics of the components necessary for operation, is shown in Fig. 2.11. The fluid that is transferred from above the piston to below (and vice versa) must pass through the MR valve. The MR valve is a fixed-size orifice with the ability to apply a magnetic field, using an electromagnet, to the orifice volume. This magnetic field results in a change in viscosity of the MR fluid, causing a pressure differential for the flow of fluid in the orifice volume. The pressure differential is directly proportional to the force required to move the damper rod. As such, the damping characteristic of the MR damper is a function of the electrical current flowing into the electromagnet. This relationship allows the damping of an MR damper to be easily controlled in real time.

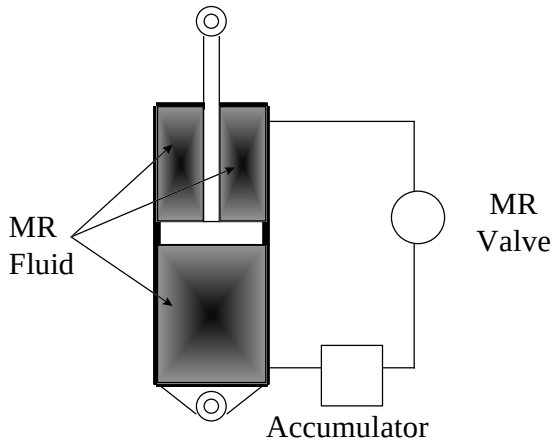

Figure 2.11. Functional Representation of an MR Damper

The accumulator is a pressurized volume of gas that is physically separated from the MR fluid by a floating piston or bladder. The accumulator serves two purposes. The first is to provide a volume for the MR fluid to occupy when the shaft is inserted into the damper cylinder. The second is to provide a pressure offset so that the pressure in the low pressure side of the MR valve does not induce cavitation in the MR fluid by reducing the pressure below the vapor pressure of the MR fluid.

The design of the MR damper developed by Lord Corporation, Koni Incorporated, and the Advanced Vehicle Dynamics Laboratory at Virginia Tech is shown in Fig. 2.12. All of the external components have been incorporated internally, providing a compact design that is very similar in size and shape to existing passive vehicle dampers. The only external parts are the two electrical leads for the electromagnet, which are connected to the current source.

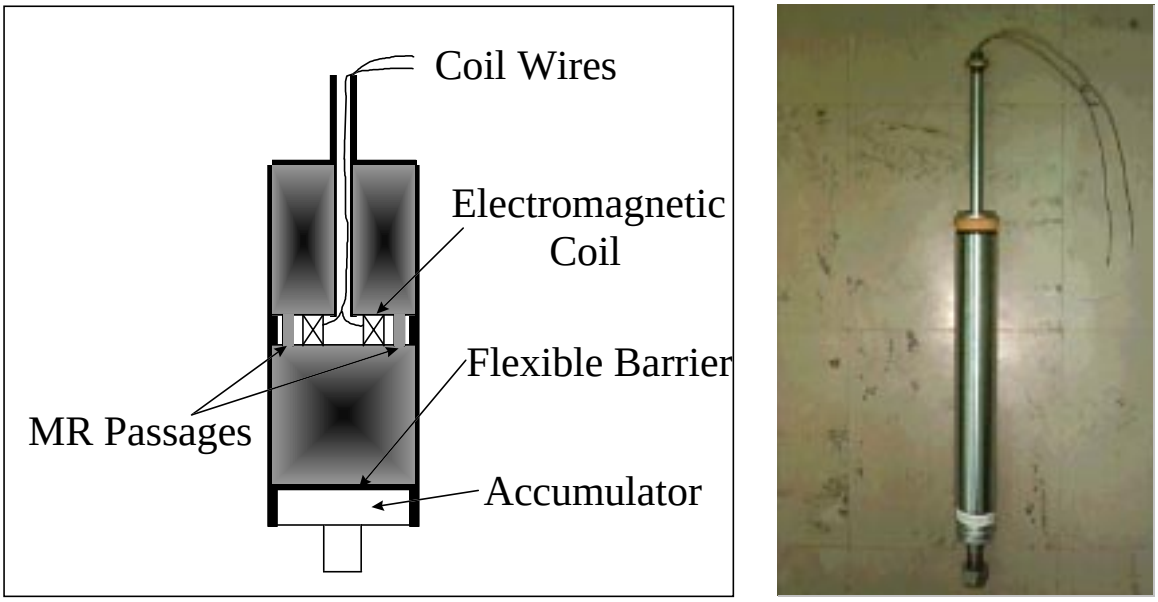

(a) (b)

Figure 2.12. Lord/Koni MR Damper, (a) Schematic Representation, (b) Actual Hardware

2.3.3 Performance of the MR Damper

For typical passive dampers, the damper performance is often evaluated based on the force vs. velocity characteristics. For a linear viscous damper, the force vs. velocity performance is shown in Fig. 2.13. The slope of the force vs. velocity line is known as the damper coefficient, C. In practice, however, the force vs. velocity line is frequently bilinear and asymmetric, with a different value of C for jounce (compression) and rebound (extension), as shown in Fig. 2.14. The reason for having asymmetric damping characteristics stems from the final application of the damper in a vehicle suspension. When working in series with the primary spring of the vehicle suspension, the damper is working against the spring force in compression and is greatly aided by the spring force in rebound. If the vehicle encounters a pothole or momentary loss of contact with the road, the only mechanism preventing the suspension from rebounding to the physical stops is the rebound damping [26].

Since the characteristics of a passive damper are such that there is only one force corresponding to a given velocity, the damping curve is tuned by a ride engineer for each particular application. Therefore, the operational envelope of a passive damper is confined to one pre-designed force-velocity characteristic.

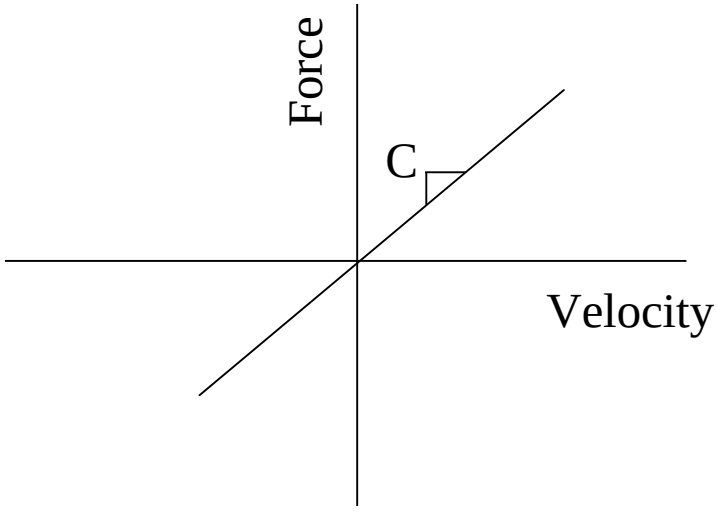

Figure 2.13. Linear Damper Characteristics

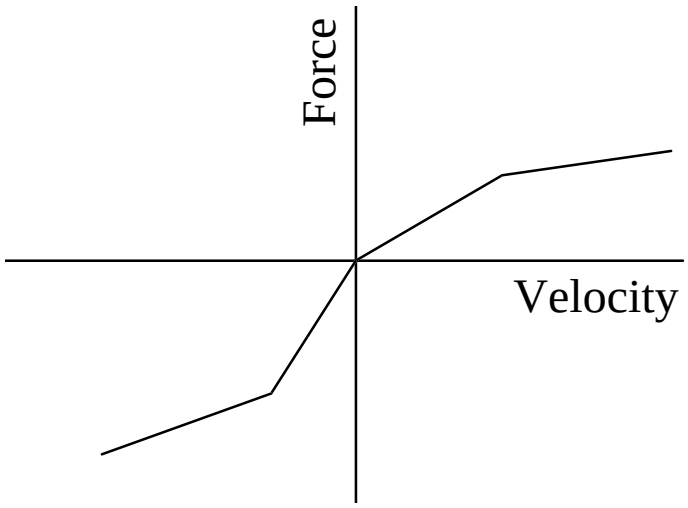

Figure 2.14. Bilinear, Asymmetric Damping Characteristics

In the case of MR dampers, the ideal force-velocity characteristics are as shown in Fig. 2.15. The result is a force vs. velocity envelope that is spanned by an area rather than a line in the force-velocity plane. In this ideal case, the damper force is independent of the shaft velocity, and is only a function of the current going into the coil. Effectively, the controller can be programmed to emulate any damper force-velocity characteristic or control policy within the envelope.

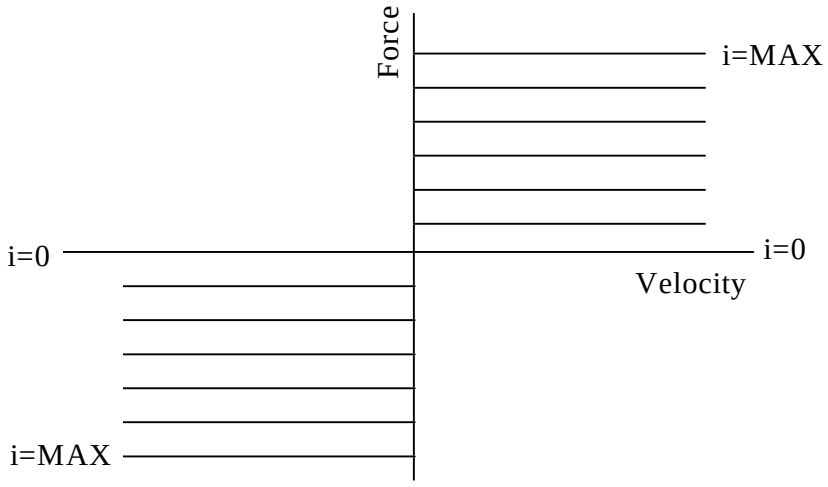

Figure 2.15. Ideal MR Damper Performance

We can model the ideal MR damper according to

$$F_{MRDAMPER} = \alpha i \tag{2.10}$$

where α is a constant and i is the damper current. Figure 2.16 shows the actual nonlinear force-velocity characteristics for the MR damper used for this research. The model in Eq. (2.10) and Fig. 2.15 does not capture the fine details of the actual MR damper; some of the effects missing from the model include the magnetic field saturation, hysteresis, and the force due to the pressurized accumulator. As will be shown in later chapters, this approximation is sufficient for designing MR dampers for most applications, including vehicle suspensions.

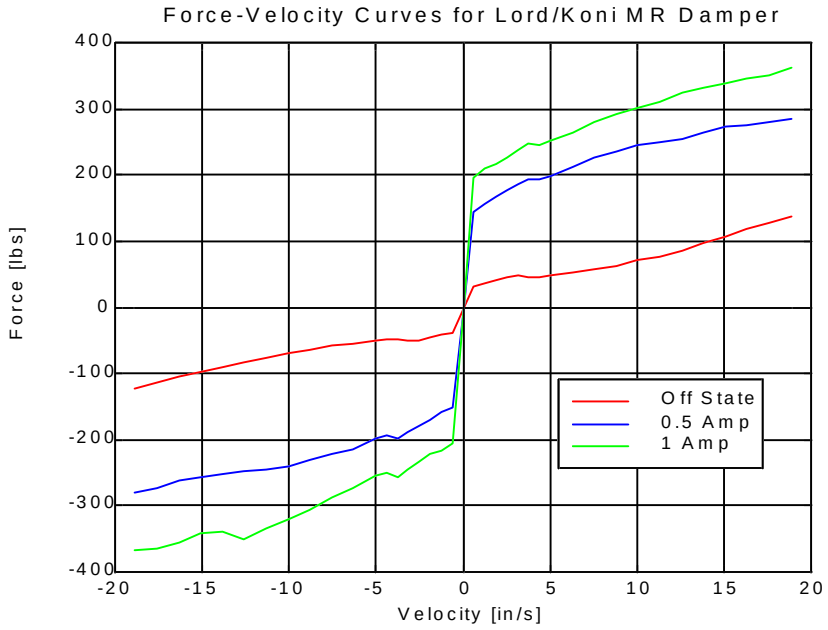

Figure 2.16. MR Damper Performance Envelope

Chapter 3

Experimental Setup

This chapter describes the experimental setup of the quarter-car test apparatus used for laboratory testing at the Advanced Vehicle Dynamics Lab (AVDL) at Virginia Tech. First, the structural design of the quarter-car test apparatus will be discussed. Next, the actuation system used to excite the quarter-car will be discussed, followed by a description of the actual excitation signals used to excite the quarter-car. The sensory information gathered and the data acquisition system used will then be detailed. The development of the control system for the MR dampers will be discussed, and finally a description of the Lord/Koni MR damper used for this research will be presented.

3.1 Structural Design of the Quarter-Car Test Apparatus

The MR dampers used in this research were tested on a specially-designed 2DOF quarter-car test apparatus that closely resembles a single suspension system from a passenger vehicle. The quarter-car apparatus is shown in Fig. 3.1. The structure is formed from extruded aluminum manufactured by 80/20 Inc. The extruded T-shaped profiles of the 80/20 stock facilitate easy joining and bracing of the structure. The main structure consists of four upright 3”x3” posts (approximately 84” tall) fastened with angle brackets to a 36”x36”x0.75”-thick steel plate, which in turn is anchored with lag bolts to the concrete floor.

One key design specification for the quarter-car is that it must be stiff enough in all modes so that the first natural frequency of the structure itself is not in the range of frequencies to be measured. Having the first mode natural frequency below 25 Hz is not acceptable, as base excitation energy will go into the structure, unmeasured, rather than into the sprung and unsprung masses. This unmeasured energy will corrupt the necessary

output data, resulting in a low coherence function from input to output. For this reason, every effort was made to make the structure as stiff as possible in the three modes deemed to be the most critical: fore/aft towering of the vertical structure, side-to-side towering of the vertical structure, and torsional bending of the structure about a vertical axis in the center of the structure.

To combat side-to-side towering of the quarter-car, diagonal braces were installed to triangulate the structure. These braces raised the side-to-side vibration frequency well over the desired level of 25 Hz. In addition, the diagonal braces added the necessary torsional rigidity to the structure to nearly eliminate torsional bending. Fore/aft towering, however, was not reduced significantly because the triangulating braces added ran only from left to right, not fore to aft. The fore/aft towering mode natural frequency was still about 8 Hz, an unacceptable value. Braces could not be added fore and aft on the structure because they would directly interfere with the free vertical motion of the sprung and unsprung masses. A solution was found by anchoring the top of the structure to a concrete wall directly behind the quarter-car. This horizontal brace increased the fore/aft stiffness of the quarter-car greatly, effectively raising the last critical natural frequency of the structure to well over 25 Hz.

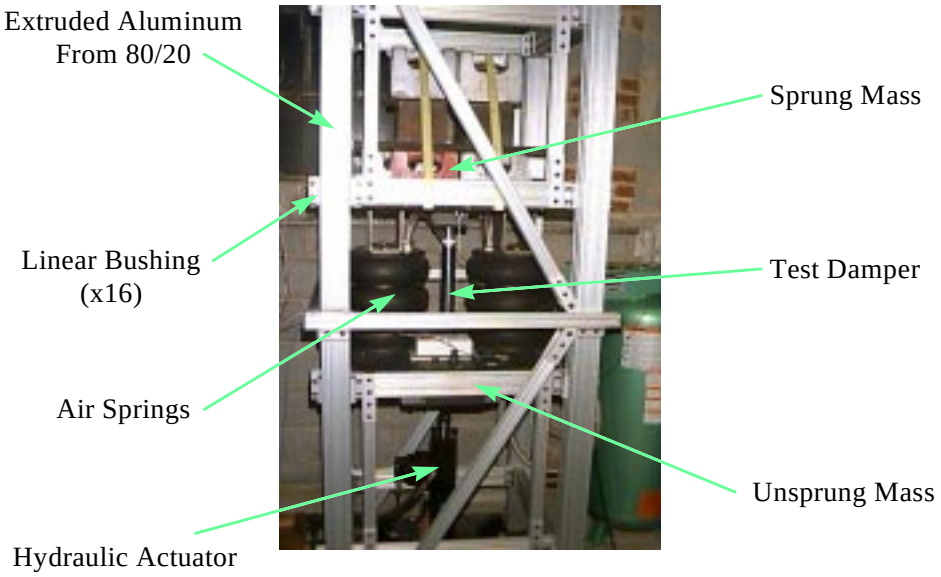

Figure 3.1. Virginia Tech AVDL Quarter-Car Test Apparatus

The main components of the quarter-car test apparatus are derived directly from the 2DOF quarter-car model in Fig. 2.1. The unsprung mass is attached to the main structure via eight teflon-padded linear bushings that slide on the four main posts. A close-up of one of these bushings is shown in Fig. 3.2. To prevent binding of the linear bushings, there are two sets of four bushings placed 20" apart to handle any side loading and increase the L/D factor which prevents binding. The unsprung mass of a typical passenger vehicle is approximately 30 kg or 70 pounds. The unsprung mass sub-structure weighs approximately 70 pounds as is, so no additional weight needs to be added or removed to accurately model the unsprung mass of a vehicle.

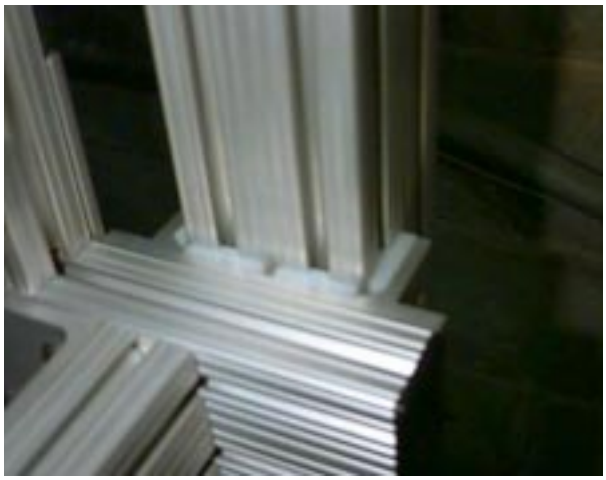

Figure 3.2. Linear Bushing

The unsprung mass is excited by an MTS hydraulic actuator through eight elastomeric mounts manufactured by Lord Corporation. The stiffness of each mount is such that when eight are placed in parallel, their combined stiffness adds to a value closely resembling an actual tire vertical stiffness (at a reasonable tire pressure). The arrangement of the elastomeric mounts is shown in Fig. 3.3. The mounts are installed so that they are flexed in their shear axes to limit the amount of radial motion that the actuator experiences. Since the mounts are about five times stiffer in compression versus shear, mounting them in shear forces the actuator to transmit only vertical excitations to the structure.

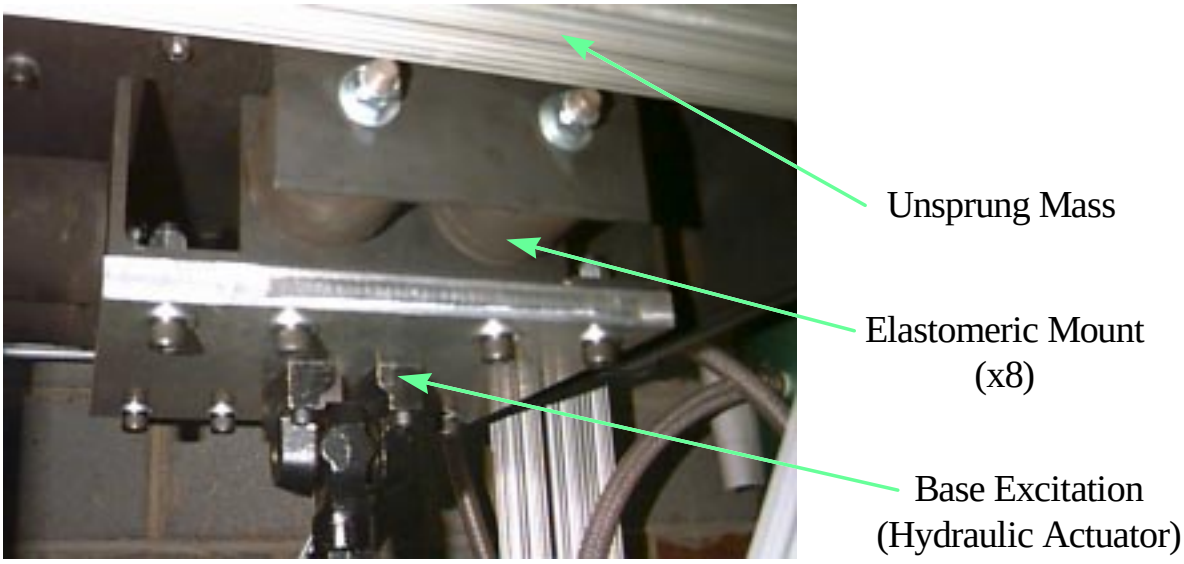

Figure 3.3. Quarter-Car Tire Stiffness

The sprung mass DOF is similar in construction to the unsprung mass DOF. The sprung mass is also attached to the main posts via eight linear bushings so that it may translate freely in the vertical direction. The sprung mass sub-structure has approximately 700 pounds of dead weight fastened to it to simulate one quarter of the sprung mass of a typical vehicle. The dead weight consists of 50-pound blocks fastened to the sprung mass sub-structure with tie-down straps. The sprung mass is coupled to the unsprung mass with two airsprings and a damper, which together simulate the primary suspension of a vehicle. The sprung mass DOF is shown in Fig. 3.4.

Figure 3.4. Sprung Mass DOF

To model the primary spring of a vehicle, two airsprings are mounted in parallel and attached to both the sprung mass above and the unsprung mass below. Airsprings were chosen to model the primary spring because their stiffness is adjustable based on the internal pressure of the airspring. In the laboratory testing environment, it is favorable to have an adjustable spring not only so that the exact stiffness can be achieved, but also so that many different vehicles can be simulated with the quarter-car apparatus. A sealed airspring by nature is highly non-linear, with the spring rate rapidly rising when the spring is compressed. Since the spring rate for an airspring is a function of the internal pressure of the airspring, the rising rate is due to the increase in pressure resulting from a decrease in the volume of the compressed airspring. To eliminate this problem, the two airsprings on the quarter-car are connected via ¾" braided hose to a 30-gallon air tank (Fig. 3.5) which acts as a reservoir volume to effectively maintain near constant pressure throughout the closed air system.

Figure 3.5. Constant Pressure Air Reservoir

In practice, the internal pressure, and thus the spring rate, is observed to be nearly constant. When the internal pressure of the tank (and thus the airsprings) is 12.5 psi, the resultant airspring stiffness is 100 lb/in, a value that is very near one-half of the spring constant for a typical vehicle primary spring. When two airsprings are put in parallel, the resultant spring constant accurately models the physical vehicle.

The test damper for the quarter-car is mounted in the center of the structure in a parallel configuration with the two airsprings. Since the spring force can be quite different from the damper force, the structure is kept balanced by mounting the damper in the center with the two airsprings symmetrically located on either side. This arrangement is shown in Fig. 3.6.

Figure 3.6. Primary Suspension Envelope

3.2 Actuation System

In order to excite the suspension system as if it were mounted in a vehicle, a hydraulic actuation system consisting of a hydraulic pump, manifold, and actuator was mounted to the quarter-car structure. The hydraulic system is manufactured by Materials Testing

System (MTS). A Hydraulic Power Supply, Model 502.020, similar to the one shown in Fig. 3.7, was used to provide fluid to the manifold at the rate of 6 gallons per minute (GPM or 24 *l*/min) with 3000 psi (21 MPa) pressure.

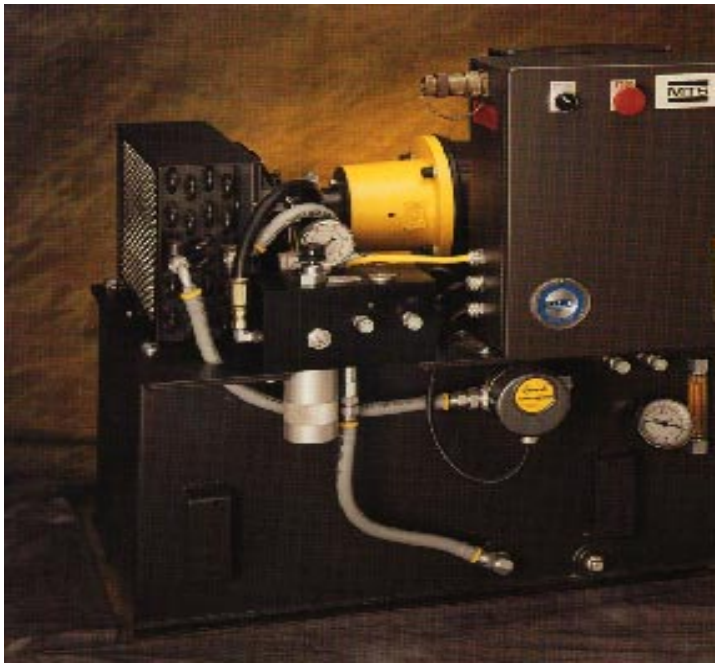

Figure 3.7. MTS 502 Hydraulic Power Supply

A Model 263 Hydraulic Service Manifold, shown in Fig. 3.8, was used to interface the hydraulic power supply to the actuator. The primary role of the manifold is to regulate the hydraulic pressure and flow to the actuator. A regulated flow is needed to ensure proper dynamic response of the hydraulic actuator.

Figure 3.8. Hydraulic Service Manifold

The Hydraulic Actuator used for this testing, shown in Fig. 3.9, is an MTS Model 242.09 actuator with ±2 inches (±5 cm) of stroke. The actuator has a force capacity of 2200 lb (10 kN), which is adequate for testing the quarter-car. The actuator is equipped with an internal load cell and linear-variable differential transformer (LVDT) for measuring actuator force and displacement, respectively. Two MTS Model 249 Swivel Ends are mounted to the actuator to correct for any misalignment between the actuator and upper and lower plates.

Figure 3.9. MTS 242 Series Hydraulic Actuator

The hydraulic system is controlled by an MTS Model 407 Controller, shown in Fig. 3.10. This controller is a single-channel, digitally-supervised, servo controller that provides complete control of the servo-hydraulic actuator. The controller can be used to prescribe a given displacement or force at the actuator.

Figure 3.10. MTS 407 Controller

3.3 Quarter-Car Apparatus Base Excitation

As stated in the previous section, the MTS 407 Controller is capable of prescribing a displacement at the actuator that tracks a voltage into the 407 Controller. For this research, a standard road surface profile consisting of white noise with frequency content from DC to 25 Hz was used [27]. The power spectrum of the input to the system is shown in Fig. 3.11.

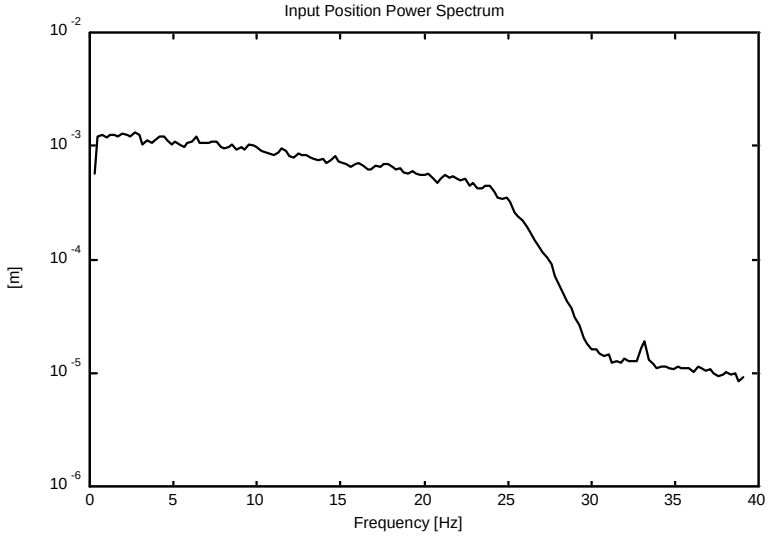

Figure 3.11. Power Spectrum of Displacement Input to the Quarter-Car System

The original input time trace is generated with a PC using MATLAB's Band-Limited White Noise block in Simulink. The time data is also low-pass filtered in Simulink, with a break frequency of 25 Hz. The filtered displacement input time trace is output from the computer via the dSPACE I/O board. The entire dSPACE system used for the input to the structure, the control of the damper, and data acquisition will be described in detail in the next section. From the PC, the signal goes to a Frequency Devices analog filter, where it is externally low-pass filtered with a break frequency of 25 Hz to ensure that there is minimal frequency content above 25 Hz entering the quarter-car structure. From the output of the filter, the signal goes to the MTS 407 Controller which then commands the hydraulic actuator to follow the prescribed displacement input. A flowchart of the displacement input generation is shown in Fig. 3.12.

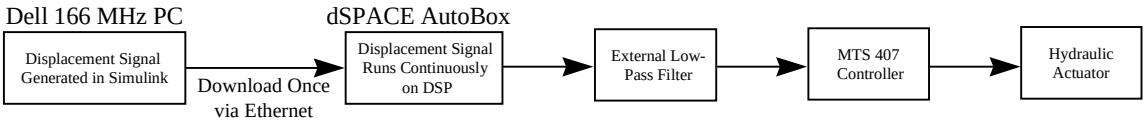

Figure 3.12. Displacement Input Generation Flowchart

3.4 Sensory Information Needed for Damper Control

This section describes the sensory information that is required to control the 2DOF quarter-car system in the three modes of skyhook, groundhook, and hybrid control. The actual sensors used will be described, and the methods for deriving the necessary physical information from the sensors on the quarter-car will be presented.

3.4.1 Sensory Information Needed for Skyhook Control

In order to identify the needed sensors, it is useful to review the requirements for skyhook control of a 2DOF suspension system. Recalling the semiactive skyhook control policy from Chapter 2,

$$\begin{cases} V_1 V_{12} > 0 & F_{SA} = C_{SKY} V_1 \\ V_1 V_{12} < 0 & F_{SA} = 0 \end{cases} \tag{3.1}$$

where:

V_1 = absolute velocity of the sprung mass with respect to the ground

V_{12} = relative velocity between the sprung and unsprung masses

F_{SA} = semiactive damping force

C_{SKY} = skyhook damping coefficient

One method for determining the absolute velocity of the sprung mass and the relative velocity between the sprung and unsprung masses would be to derive the values from accelerometer signals. One accelerometer could be placed on the sprung mass, and the other on the unsprung mass. The acceleration signals could then be integrated, either digitally or with an analog integrator, to obtain the corresponding velocity signals. Since an accelerometer is an inertial sensor, the velocities resulting from the integration would be inertial in nature (i.e. with respect to a fixed ground). We would then have V_1 measured directly, and we could take the difference between V_1 and V_2 (i.e. V_1-V_2) to determine the relative velocity, V_{12}.

For skyhook control, the velocity of the sprung mass V_1 must be measured with respect to ground, so the integrated accelerometer approach is necessary. A Texas Instruments Model CAS capacitive DC accelerometer, shown in Fig. 3.13, is used for this purpose. The CAS is designed for automotive applications, so it is compact and rugged. This device is easy to use because it contains onboard signal conditioning that converts the sensing element capacitance directly to a voltage.

Figure 3.13. Texas Instruments CAS Accelerometer

The unsprung mass absolute velocity, V_2, does not need to be sensed directly for skyhook control; in this scenario, it is used only to indirectly measure V_{12}. A much cleaner way of determining the relative velocity is to measure it directly. A UniMeasure Model VPA-10 Velocity-Position Transducer, shown in Fig. 3.14, is connected between the sprung and unsprung masses on the quarter-car to measure V_{12} directly.

Figure 3.14. UniMeasure VPA-10 Velocity-Position Transducer

The UniMeasure VPA-10 transducer works well in the laboratory setting, but for in-vehicle application of skyhook control, this transducer would not be applicable due to its size. The best technique for measuring V_{12} on a vehicle would be to either utilize the two-accelerometer approach mentioned above, or numerically differentiate the signal from a relative displacement transducer such as a linear potentiometer.

3.4.2 Sensory Information Needed for Groundhook Control

As stated in Chapter 2, the groundhook configuration is similar to the skyhook configuration, but the fixed reference damper is attached to the unsprung mass rather than to the sprung mass, resulting in the groundhook semiactive control policy

$$\begin{cases} -V_2 V_{12} > 0 & F_{SA} = C_{GND} V_2 \\ -V_2 V_{12} < 0 & F_{SA} = 0 \end{cases} \tag{3.2}$$

In this case, the sensory information needed for damper control is the absolute (inertial) velocity of the unsprung mass and the relative velocity between the sprung and unsprung masses. In a similar fashion to the skyhook semiactive control sensory information, an accelerometer is used on the unsprung mass and integrated to sense V_2, while the same UniMeasure VPA-10 transducer is used to measure V_{12}.

Typically, the acceleration transmitted to the axle (unsprung mass) of a vehicle can be on the order of 10 times higher than the sprung mass acceleration. As such, the accelerometer used to derive V_2 needs to be rated for at least 5-10 peak g's. Most DC accelerometers on the market are not capable of measuring this level of peak acceleration. PCB Piezotronics, however, manufactures a DC accelerometer, Model #370A02, that is capable of measuring accelerations of ±20g. This accelerometer is shown in Fig. 3.15. The 370A02 also has onboard signal conditioning so all that is required is an excitation voltage, and the signal is returned directly as a voltage.

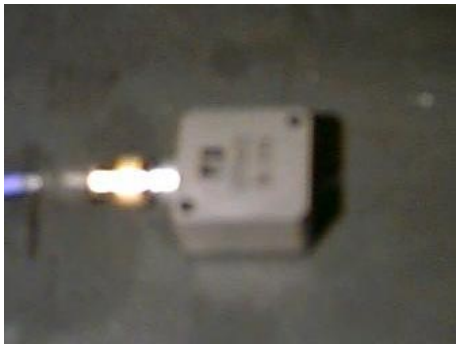

Figure 3.15. PCB Piezotronics DC Accelerometer

3.4.3 Sensory Information Needed for Hybrid Control

Consider the hybrid semiactive control algorithm from Chapter 2:

$$\begin{Bmatrix} V_1 V_{12} > 0 & \sigma_{SKY} = V_1 \\ V_1 V_{12} < 0 & \sigma_{SKY} = 0 \end{Bmatrix}$$

$$\left\{ F_{SA} = G\left[\alpha\sigma_{SKY} + (1-\alpha)\sigma_{GND}\right] \right. \tag{3.3}$$

$$\begin{Bmatrix} -V_2 V_{12} > 0 & \sigma_{GND} = V_2 \\ -V_2 V_{12} < 0 & \sigma_{GND} = 0 \end{Bmatrix}$$

Clearly, it is necessary to have an absolute (inertial) velocity measurement of both V_1 and V_2. The only way to measure both signals is to use the two-accelerometer approach. The TI CAS accelerometer is mounted on the sprung mass, and the PCB 370A02 is mounted on the unsprung mass. Since acceleration, and therefore absolute velocity, signals are available for both the sprung and unsprung masses, V_{12} can be calculated as V_1-V_2. The UniMeasure VPA-10 is used as a verification that the calculated value of V_{12} is indeed equivalent to the measured value of V_{12}.

3.5 Controller Development

This section describes the actual development and implementation of the control algorithms used to control the MR damper on the quarter-car apparatus. Also discussed are the data acquisition techniques used to record the response of the quarter-car both for the passive case and for the three different semiactive control policies.

3.5.1 dSPACE AutoBox

The physical implementation of the skyhook, groundhook, and hybrid semiactive damper control schemes is accomplished by using a dSPACE AutoBox. The dSPACE system is a powerful tool designed for rapid prototyping of controllers. The dSPACE system consists of two main elements, one in software and one in hardware.

The dSPACE software interfaces with MATLAB on a PC and allows the user to create a block diagram of the control system in Simulink, complete with inputs and outputs. The dSPACE Real-Time Interface, which runs under MATLAB, can then compile the Simulink model and load the control algorithm directly to a DSP chip in the hardware element of the dSPACE system.

The hardware portion consists of the physical AutoBox, shown in Fig. 3.16. The AutoBox contains the DSP processor board, where the control program resides, an I/O card with 20 inputs and eight outputs for sensor and actuator connections, and a power supply. The dimensions of the box are approximately 8”x10”x18”. Since the AutoBox is

designed for portable vehicle control development, the power supply consists of a DC/DC converter that allows the AutoBox to be powered directly from a vehicle 12-volt system.

Figure 3.16. dSPACE AutoBox

The dSPACE controller development system reduces the job of designing and prototyping controllers to simply building a model in Simulink and downloading the program to the AutoBox with the push of a button. The controller development process involves no assembly language programming, soldering, power conditioning, or other difficulties associated with using a microprocessor for control. Shown in Figs. 3.17, 3.18, and 3.19 are the control algorithm block diagrams for skyhook, groundhook, and hybrid control. The input and output blocks are labeled as the DS2201ADC (analog to digital converter) and DS2201DAC (digital to analog converter) and are located, respectively, at the left and right sides of the block diagram to follow the flow of the control signals. The eight ports on the output block (DAC) correspond directly to BNC connections on the AutoBox. Since the ADC has 20 inputs, the Simulink block for the ADC is broken up into five multiplexed ports that contain four inputs each. This multiplexing is done to avoid the on-screen clutter of having 20 ports on the ADC block in the Simulink model. Each of the five ports on the ADC that is in use must pass through a demultiplexer to extract the appropriate signal. For the ADC, the output of the demux block is what corresponds to the 20 input BNC's on the AutoBox.

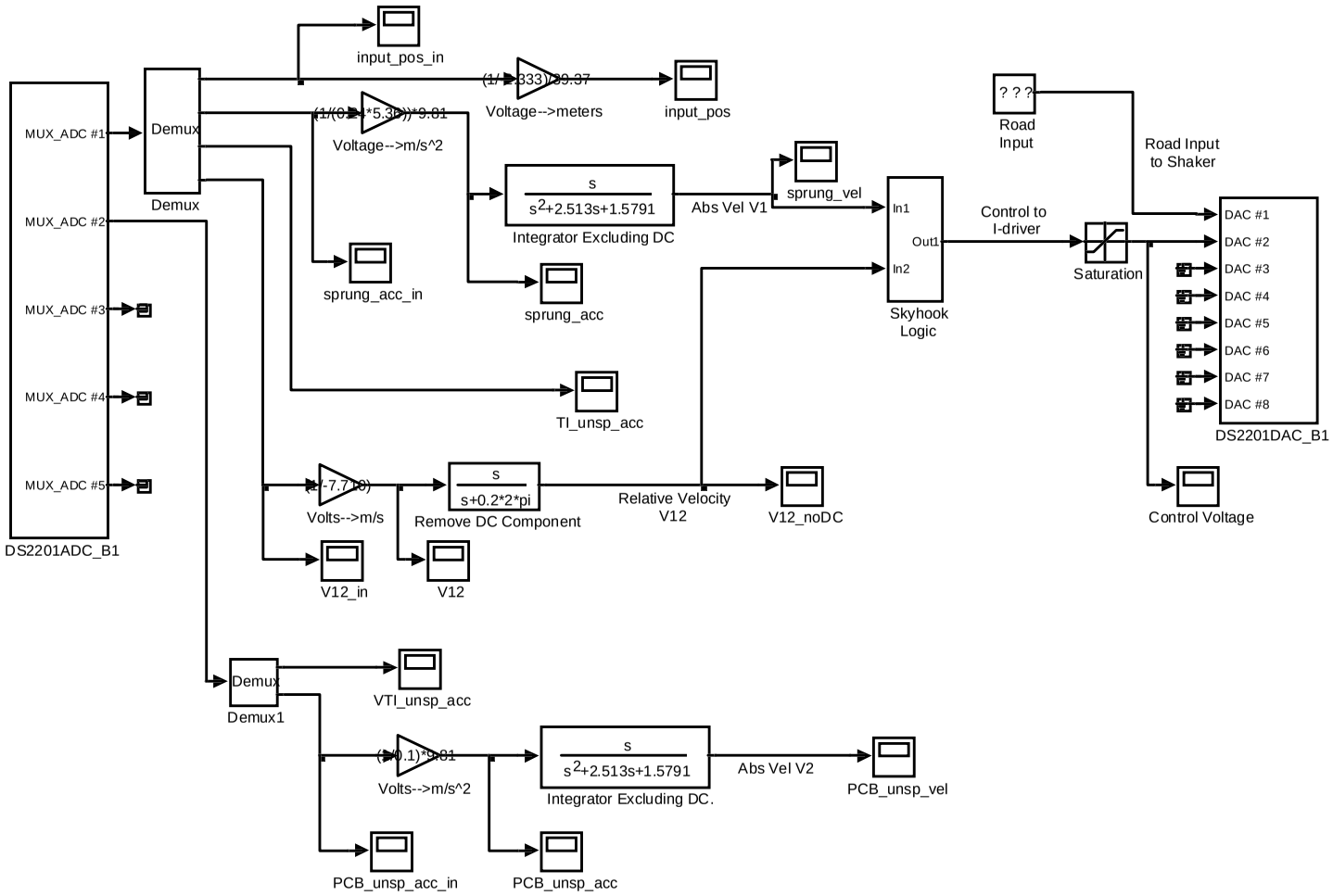

Figure 3.17. Simulink/dSPACE Control Block Diagram for Skyhook Control

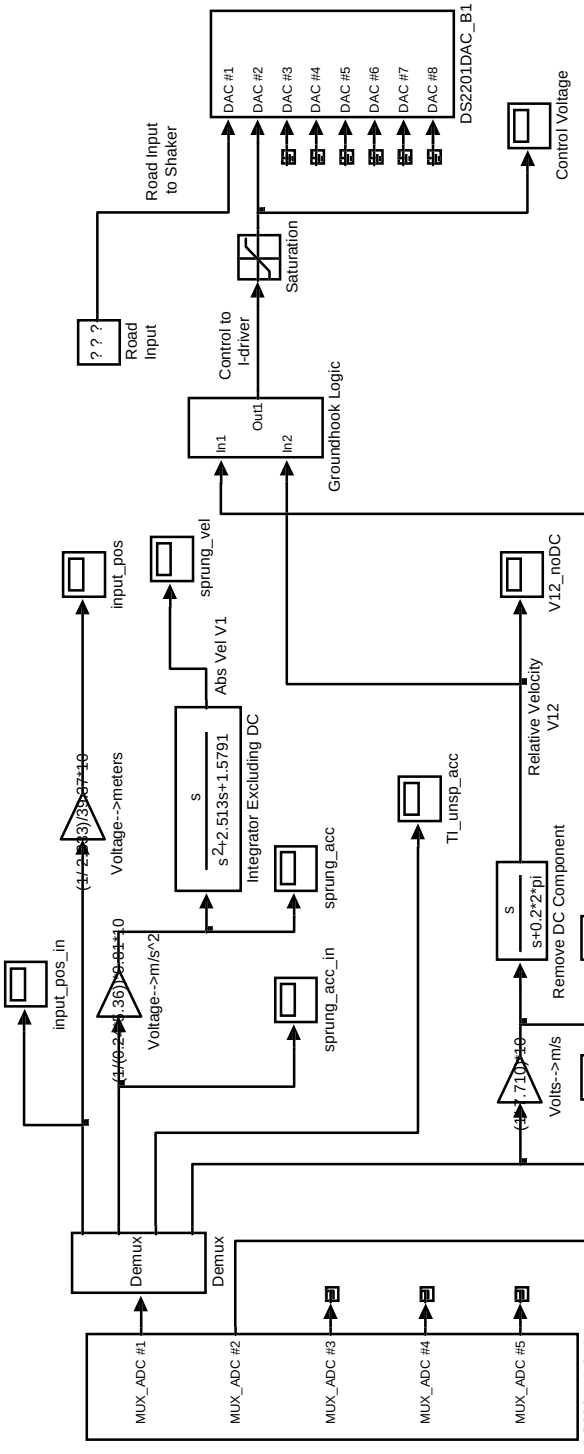

Figure 3.18. Simulink/dSPACE Control Block Diagram for Groundhook Control

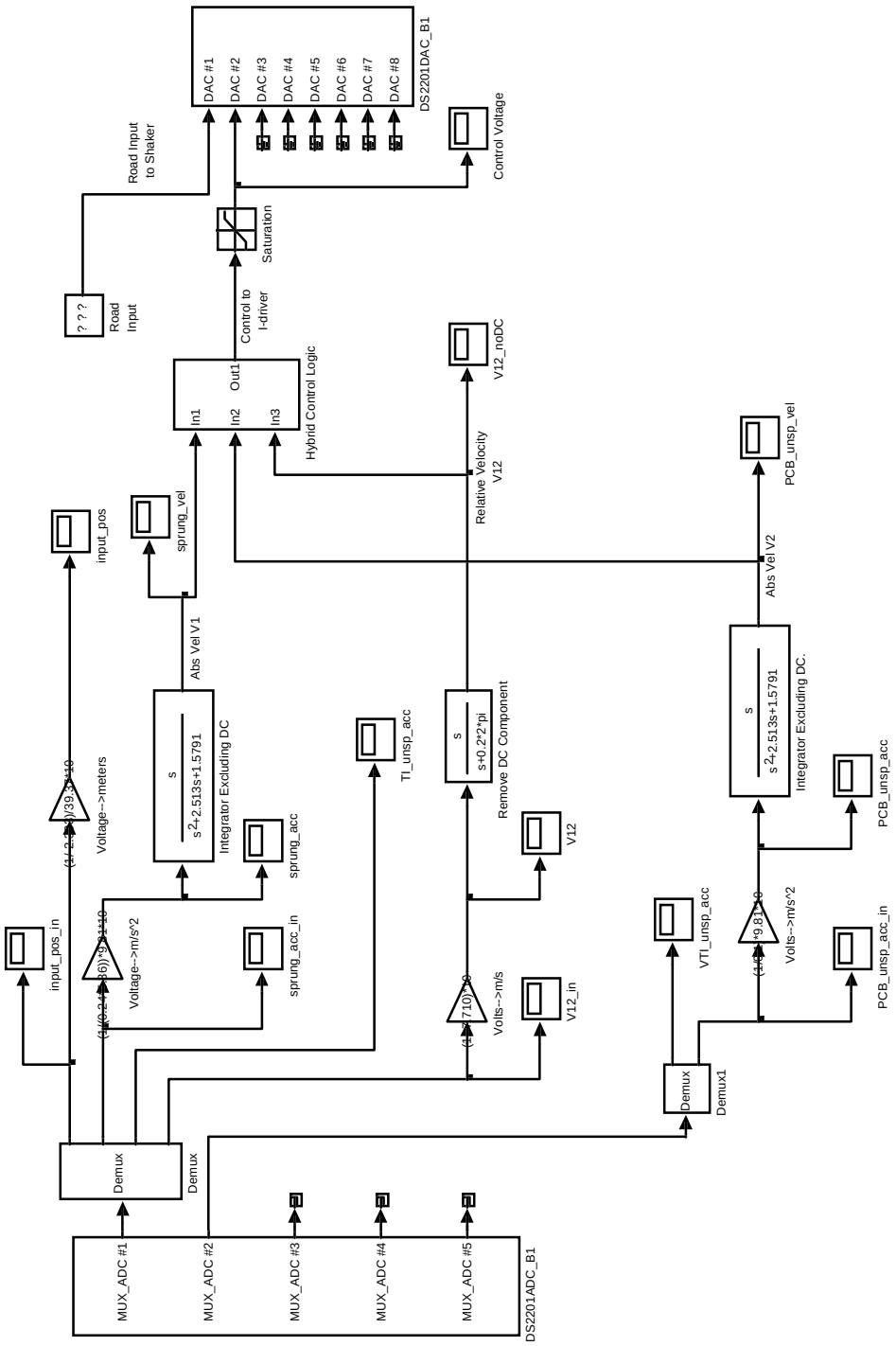

Figure 3.19. Simulink/dSPACE Control Block Diagram for Hybrid Control

The associated logic for each control scheme is contained in a masked subroutine to facilitate easier changes to the control algorithm in the model. The subroutine logic for each control scheme is shown in Fig. 3.20.

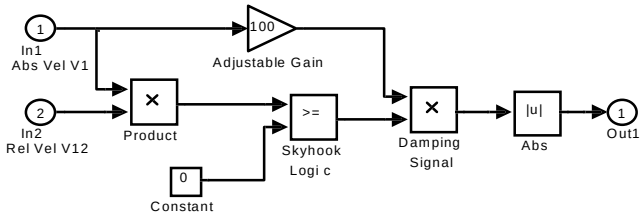

(a)

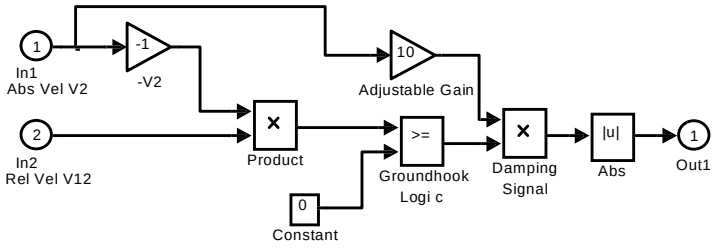

(b)

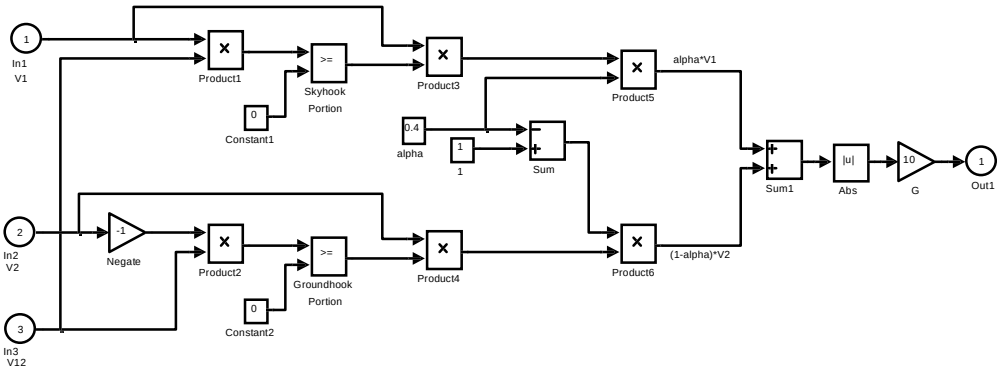

(c)

Figure 3.20. Logic Block Diagrams for (a) Skyhook Control (b) Groundhook Control (c) Hybrid Control

The nature of the sensors used for control is such that they contain a DC offset in their output voltage. These DC offsets need to be removed from the signals entering the ADC in order to accurately calculate the actual sensed value. The removal of the DC offset is accomplished by passing the signals through a high-pass filter with a break frequency of 0.2 Hz.

In the case of the accelerometer signals with DC offsets, the removal of the DC component is critical because the acceleration signals are integrated to obtain absolute velocity. If a signal with a DC offset is integrated, the value of the integral goes to infinity as $t \to \infty$. To combat this problem, the signal is passed through a transfer function of the form

$$\frac{s}{(s + 0.2 \times 2 \times \pi)^2} = \frac{s}{s^2 + 2.513s + 1.579} \tag{3.4}$$

which has one zero at $s = 0$ and two poles at $s = 0.2$. The bode plot for this transfer function is shown in Fig. 3.21. At low frequencies (i.e., $\omega < 1.2$ rad/sec or $f < 0.2$ Hz), the transfer function looks like a high-pass filter, attenuating the DC signal component. At frequencies above f = 0.2 Hz, the transfer function looks like an integrator.

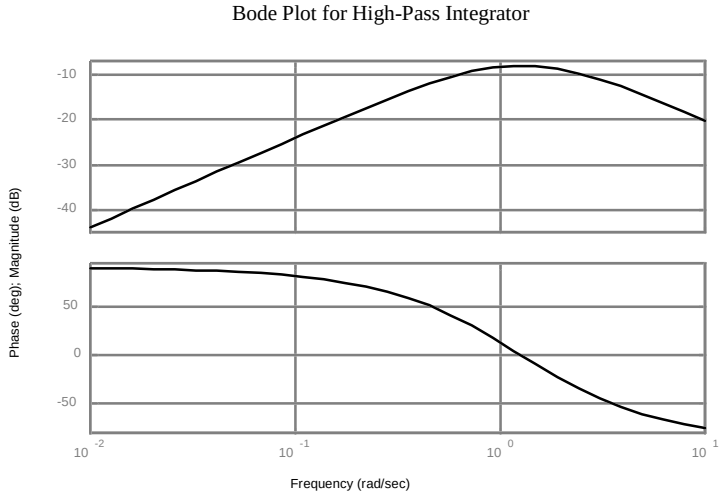

Figure 3.21. Bode Plot for Transfer Function in Eq. (3.4)

The output from channel one of the DAC is the input position signal used to base excite the quarter-car via the MTS hydraulic actuator. Although the road input file contains just three minutes of white noise, the signal is set up as a Repeating Sequence in Simulink to make the input to the structure look like continuous white noise. Having the input signal repeat in this manner facilitates the collection of time data. It is not necessary to recompile the program every time data is to be taken -- one only has to wait for the Repeating Sequence to repeat to initiate new data acquisition.

The output from channel two of the DAC is the control voltage to the MR damper. Since the MR effect is a function of the current flowing through the MR coil, a circuit needs to be used to drive a current through the damper that is proportional to the control voltage out of the dSPACE controller. The circuit shown in Fig. 3.22 is used for this purpose. The first stage of the circuit takes a voltage signal referenced to any arbitrary ground (in this case, the ground of the dSPACE controller) and converts it to a voltage referenced to the ground of the current driver circuit. The second stage of the circuit is the actual current driver, developed by Lord Corporation, that takes the voltage signal from the first stage and uses a power transistor to drive a proportional amount of current through a fixed load. In the case of the MR damper, the load is actually a coil with inductance as well as resistance, and therefore is not truly fixed. However, the inductance of the coil is small and the frequency range of interest (0-25 Hz) is low enough to neglect the effective resistance change of the load due to the time rate of change of the current.

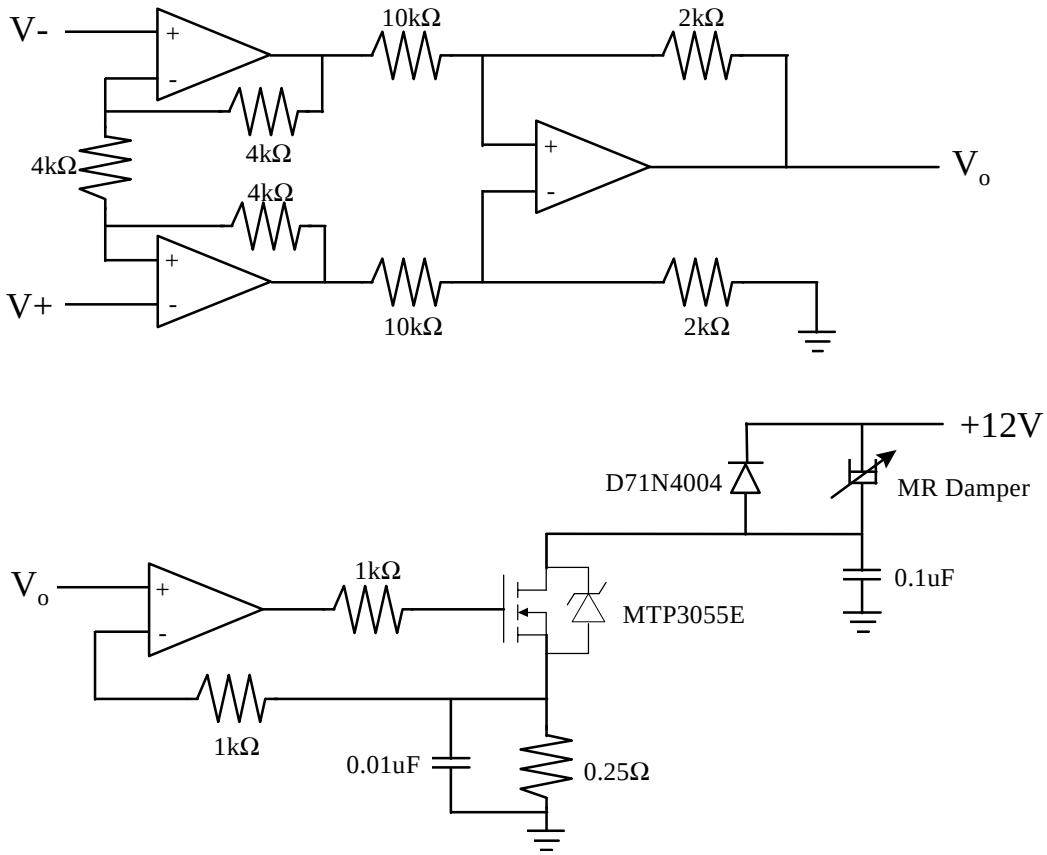

Figure 3.22. Current Driver Circuit for MR Damper

3.5.2 Data Acquisition

All data for this research were acquired directly with the AutoBox using the TRACE module in the dSPACE toolkit [28]. TRACE can generate a time history of any variable in the Simulink control block diagram. In this capacity, TRACE was used for data acquisition of all the variables contained in the "scope" blocks of the Simulink control block diagrams (input_pos, sprung_acc, sprung_vel, etc.). Figure 3.23 presents a block diagram of the data acquisition technique used. The details of the signal processing issues associated with both the sampling of the variables and the transformation from the time domain to the frequency domain are discussed in the next chapter.

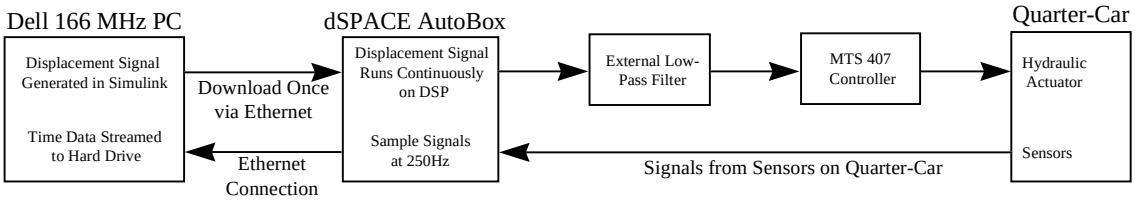

Figure 3.23. Block Diagram of Data Acquisition

Chapter 4

Results of Laboratory Testing

This chapter presents the results of the testing done with the Lord/Koni MR damper on the quarter-car test apparatus at the AVDL at Virginia Tech. The first section discusses the signal processing techniques used to analyze the time data gathered with the dSPACE TRACE program. The techniques used for generating the transmissibility plots shown in this chapter will also be presented. The next section applies these techniques to characterize the dynamic response of the quarter-car with the MR damper in two passive states. The first passive state analyzed is the off-state of the damper, and the second state is a passive on-state of the damper with 1 Amp of current flowing through the coil in the MR piston. The chapter concludes with a presentation and discussion of the experimentally determined dynamic response of the quarter-car with the semiactive MR damper running skyhook, groundhook, and hybrid control.

4.1 Signal Processing Methods

For ease of analysis of the dynamic response of the quarter-car for different passive and semiactive control strategies, the time histories of the physical parameters measured were transformed to the frequency domain. An m-file was written in MATLAB to numerically perform the signal processing operations on the time data collected with TRACE. The program loads the time data from TRACE, converts the signals from voltages to engineering units with multiplication by the sensor sensitivities, and then proceeds to the signal processing operations. First, the auto spectra of the displacement input and measured outputs of the quarter-car were calculated. The auto spectrum can be expressed as

$$G_{xx}(\omega) = \frac{2}{M}\sum_{k=1}^{M} X_k(\omega) X_k^*(\omega) \tag{4.1}$$

where $X_k^*(\omega)$ indicates the complex conjugate of the collection of frequency spectra $X_k(\omega)$. The constant M denotes the number of averages, and the factor of 2 is used for a single-sided auto spectrum. The collection of frequency spectra used to evaluate the auto spectrum were obtained by using a 1024-point Fast Fourier Transform algorithm to convert the data from the time domain to the frequency domain.

The base displacement excitation to the quarter-car is white noise, low-pass filtered at 25 Hz, as shown in Figure 4.1. Since the frequency content of the input to the system is contained below 25 Hz, it was deemed acceptable to sample the time data from the output sensors at 250 Hz. A sample rate of 250 Hz is 10 times faster than the fastest dynamics entering the system, so aliasing in the measured signals of frequency content higher than the Nyquist frequency of 125 Hz is not an issue. This sample frequency was also selected to give a reasonable frequency resolution in the frequency domain. Using a 1024-point FFT with $f_s = 250\,\text{Hz}$ results in a frequency resolution of approximately ¼ Hz.

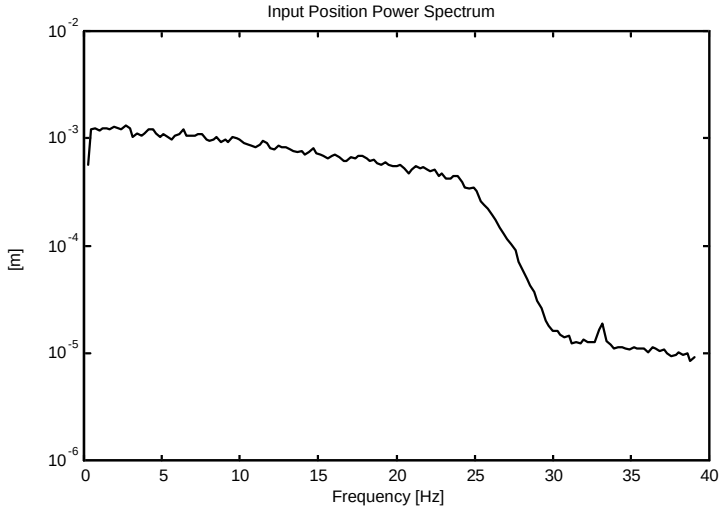

Figure 4.1. Base Displacement Input to Quarter-Car

The m-file code used to perform the signal processing operations on the time data is structured such that the entire block of data is broken up into N number of individual blocks, each 1024 points long. A 50% overlap is used on the time data to increase the number of averages calculated. An algorithm to determine the actual number of averages is shown as Eq. (4.2), where *n_sig* is the total number of points in the time history, *n_fft* is the number of points used to evaluate the FFT (1024 in this case), and *overlp* is a user-defineable number from 0 to 1 which defines the overlap percentage.

```
n_average = fix((n_sig/n_fft - overlp)/(1-overlp))
```
(4.2)

A "For" loop is used to evaluate the frequency domain results for each average. To prevent spectral leakage, each time through the loop, the current block of 1024 points is multiplied by a Hanning window. Applying a Hanning window ensures that the resulting block of time data is periodic in the 1024-point window, having both a magnitude and slope of 0 at the endpoints.

The same basic programming principles are used to evaluate frequency response functions (FRF's) from the input displacement to the output response of the quarter-car apparatus. The H_1 FRF estimator used in this work is shown below,

$$H_1 = \frac{G_{xy}}{G_{xx}} = \frac{X^*(\omega)Y(\omega)}{X^*(\omega)X(\omega)} \tag{4.3}$$

where G_{xy} is the cross spectrum from input to output, and G_{xx} is the auto spectrum of the input as described in Eq. (4.1). To evaluate H_1, it is clear that two signals must be passed into the loop and manipulated for each average (versus only one signal in the case of the auto spectrum). Of particular interest for this research are the displacement transmissibilities from the input to the output of the sprung mass and from the input to the output of the unsprung mass. The output sensors, however, measure the acceleration of the sprung and unsprung masses. To calculate the displacement transmissibility, the H_1

FRF is divided by $(j\omega)^2$ in the frequency domain to convert from acceleration over displacement to displacement over displacement.

4.2 Characterization of the Lord/Koni MR Damper

This section presents the results of baseline testing of the quarter-car with the MR damper installed and operating in a passive state. The dynamic response of the system is evaluated with the MR damper in the off-state (no current to the MR piston coil) and in the on-state. Two on-state passive damping scenarios are presented, one with 0.5 Amps flowing through the MR coil, and one with 1 Amp flowing through the MR coil.

4.2.1 Off-State Passive Case

The off-state (zero current) force-velocity curve for the Lord/Koni MR damper is shown in Fig. 4.2. This plot displays the typical bilinear force-velocity characteristic of an automotive damper.

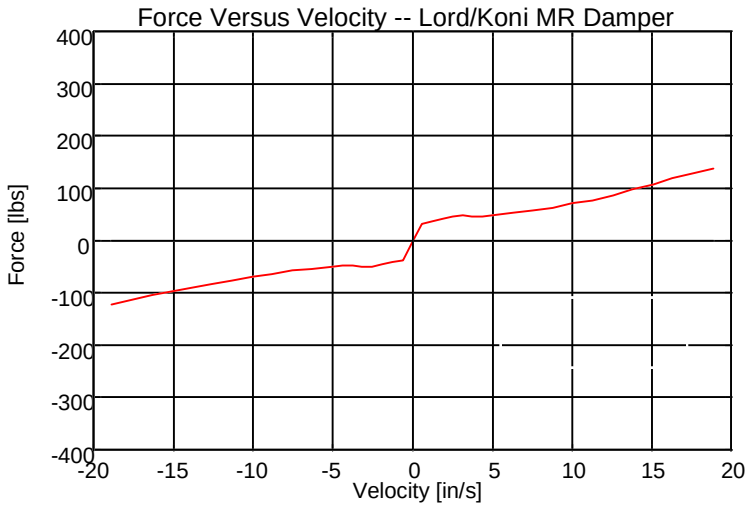

Figure 4.2. Measured Off-State Force-Velocity Curve of the MR Damper

The damping that is present in the off-state is primarily a function of the fixed orifice in the damper piston. The orifice size of the MR damper is one of many variables

that the designer of the MR damper has to specify. A large orifice will yield a low and flat off-state force-velocity curve. Recall from Chapter 2 that the ideal skyhook and groundhook configurations have an off-state damping force of zero. For this reason, it is desirable to have a large orifice in the MR piston to reduce the off-state damping force as much as possible. Having a large orifice, however, limits the damping force that is attainable in the highest on-state. Basically, the characteristic force-velocity envelope of an MR damper is roughly the same size regardless of the orifice size. Thus, the only implication of a different orifice size is a vertical offset of the force-velocity envelope, with the amount of offset determined by the highest damping force required.

The experimentally determined off-state transmissibility of the quarter-car is shown in Fig. 4.3 for both the sprung and unsprung masses.

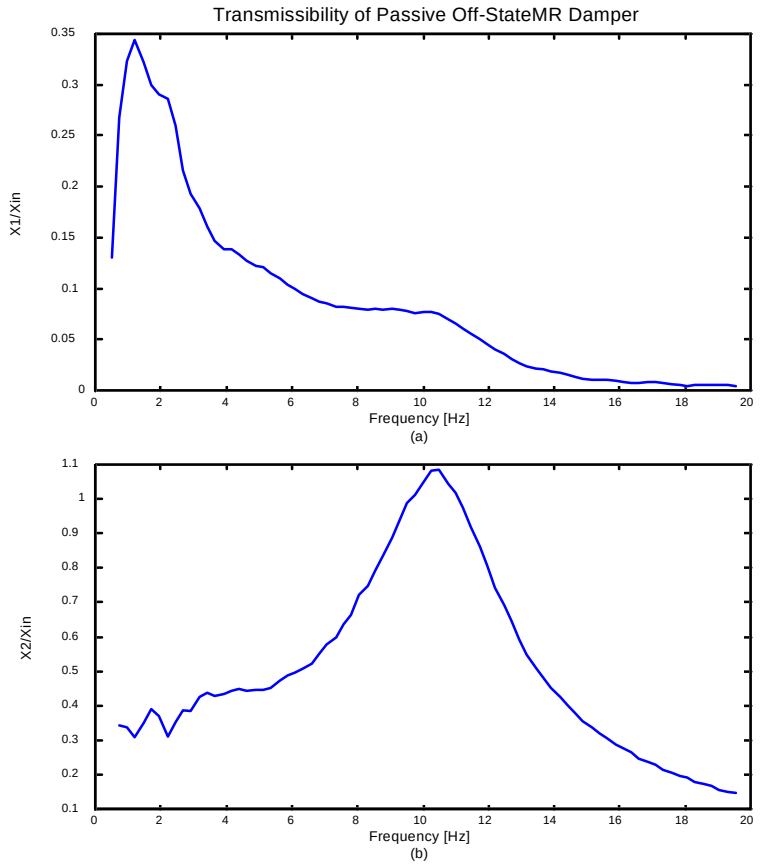

Figure 4.3. Off-State Passive Transmissibility for Quarter-Car System
(a) Sprung Mass Transmissibility (b) Unsprung Mass Transmissibility

As expected, the transmissibility plots for the quarter-car with off-state passive damping resemble the ideal transmissibility plots for the quarter-car model shown in Fig. 2.2. The damped sprung mass natural frequency can be identified at approximately 1.7 Hz, and the unsprung mass natural frequency can be identified at approximately 10.5 Hz. These frequencies are typical of a standard passenger vehicle's body and axle-hop frequencies.

4.2.2 On-State Passive Case

Figure 4.4 shows the experimentally determined force-velocity relationship for the MR damper in two on-states in addition to the off-state. The two passive on-states used were 0.5 Amp and 1 Amp flowing through the MR coil. Near 1 Amp, the MR coil begins to experience magnetic saturation, where the force-velocity relationship does not change significantly with increasing current.

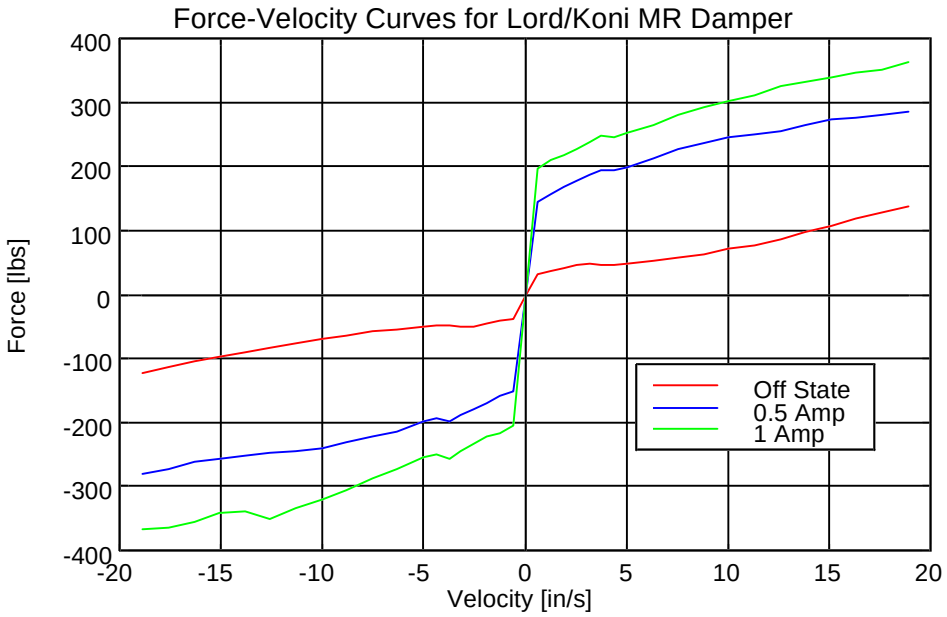

Figure 4.4. Force-Velocity Curves for Several Current Levels

The experimentally measured transmissibilities for several passive cases are shown in Fig 4.5. The effects of the shift in the resonant frequency due to the increased

coupling of the two masses are apparent at higher damper currents. Notice that the X_1/X_{in} and X_2/X_{in} plots for the 1-Amp case are nearly identical. In essence, the MR damper can effectively be locked out (to become a rigid link) at high current levels. Both plots for 1 Amp are showing the response of the sprung and unsprung masses, coupled as a near rigid body, vibrating as a single-degree-of-freedom system on the tire stiffness.

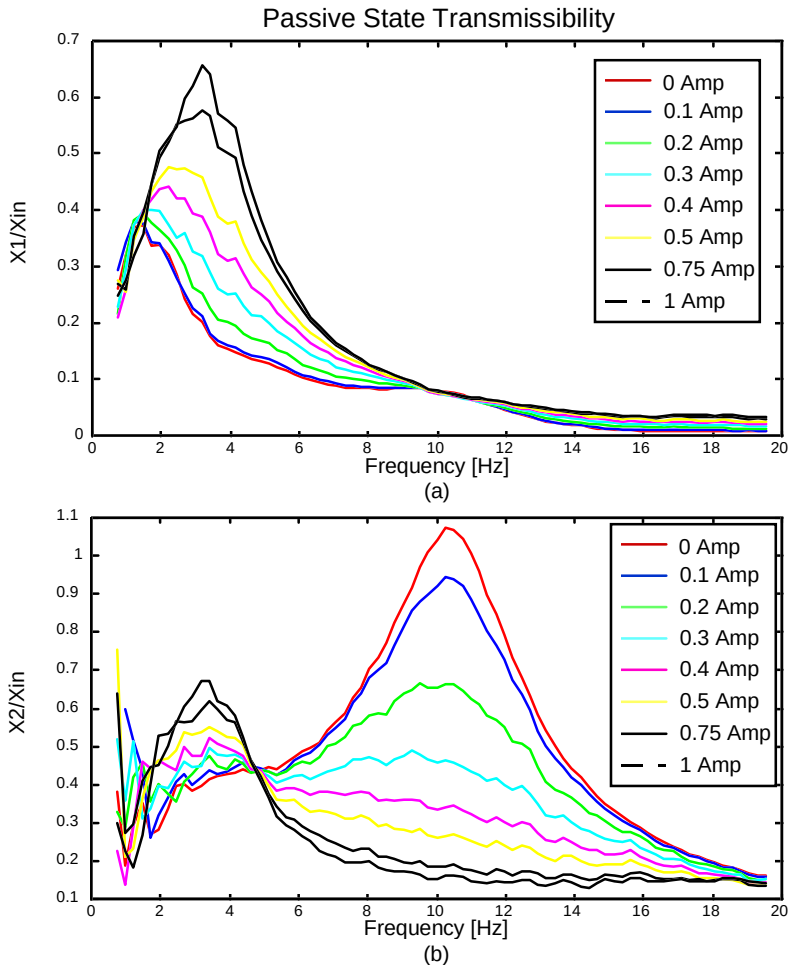

Figure 4.5. Passive Transmissibility of Quarter-Car for Different Damper Currents
(a) Sprung Mass Transmissibility (b) Unsprung Mass Transmissibility

Figure 4.6 shows a time trace of the sprung mass acceleration for the three cases of passive damping. Higher levels of sprung mass acceleration are present with more current to the MR coil (i.e., a stiffer damper). The human body objects to vertical

accelerations in the neighborhood of 2.5 m/s^2 and higher, so clearly the 0.5 and 1 Amp cases would be unacceptable from the standpoint of ride comfort.

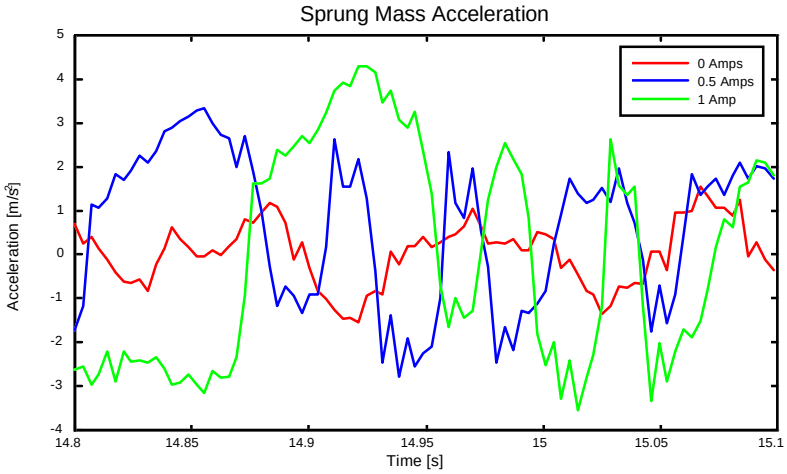

Figure 4.6. Sample Time Trace of Sprung Mass Acceleration

Effectively, more energy from the base excitation is being transmitted through the primary spring and damper and into the sprung mass. This observation re-illustrates the fundamental problem with passive suspensions, specifically the lack of isolation that comes with increased passive damping.

4.3 Effects of Semi-Active Control on Dynamic Response

This section discusses the effects that the different control schemes of skyhook, groundhook, and hybrid semiactive control have on the dynamic response of the 2DOF system. The data gathered from the quarter-car are analyzed in both the time domain and the frequency domain. The data are examined in the time domain to verify that the control signal to the MR damper is in accordance with the control scheme being used. The data are examined in the frequency domain to investigate the dynamic response of the system when the control parameters are changed.

4.3.1 Skyhook Control

Recall from Chapter 2 that skyhook control attempts to minimize sprung mass motion at the expense of unsprung mass motion. The skyhook control law is described by

$$\begin{cases} V_1 V_{12} > 0 & F_{SA} = C_{SKY} V_1 \\ V_1 V_{12} < 0 & F_{SA} = 0 \end{cases} \tag{4.4}$$

A section of the time trace of the sprung mass absolute velocity (V_1) in m/s^2, the relative velocity (V_{12}) in m/s^2, and the damper current in Amps is shown in Fig. 4.7. The current driver has a sensitivity of 0.15 Amps/Volt, so the peak control voltage is limited to 7 Volts, which corresponds to a peak MR damper current of approximately 1 Amp. Since the time histories of the variables were captured from the Simulink model using the TRACE module, a factor of 10 needs to be applied to the variables for them to have physical meaning. Zero to 10 Volts at the input to the A/D converter corresponds to a number from 0 to 1 in the Simulink code. Similarly, a number from 0 to 1 in the Simulink code corresponds to a voltage from 0 to 10 at the output of the D/A converter.

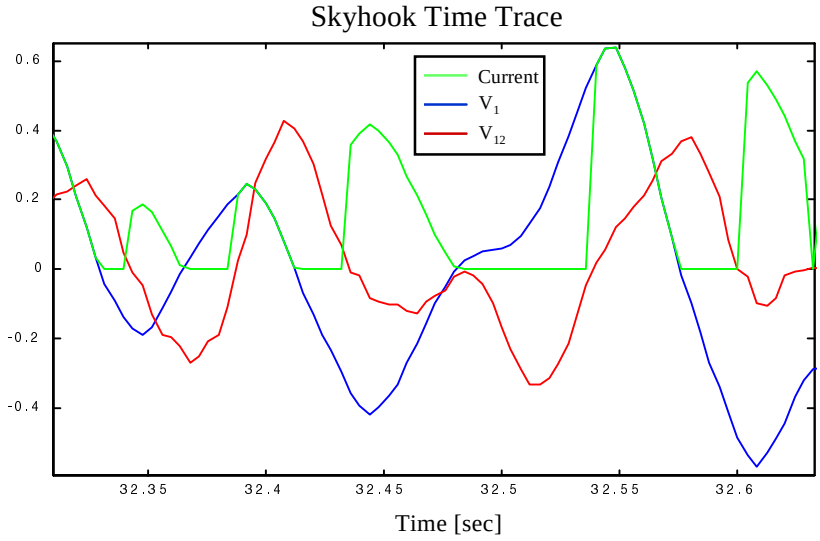

Figure 4.7. Sample Time History of Variables for Skyhook Control

By examining the time trace of V_1, V_{12}, and the damper current, we can see that the skyhook control policy is indeed being executed. When V_1 and V_{12} have the same

sign, the control signal is on and proportional to V_1, whereas when V_1 and V_{12} have different signs, the control signal is off.

To understand the 2DOF dynamics of the quarter-car under semiactive skyhook control, it is necessary to look at the transmissibility of the sprung and unsprung masses with respect to the input. These transmissibility plots are shown in Fig. 4.8 for various values of the skyhook gain, G (effectively C_{sky}). Increasing skyhook damping results in a reduction in amplitude at the sprung mass natural frequency, with a corresponding increase in amplitude at the unsprung mass natural frequency. In addition, the isolation at higher frequencies improves with increased skyhook damping.

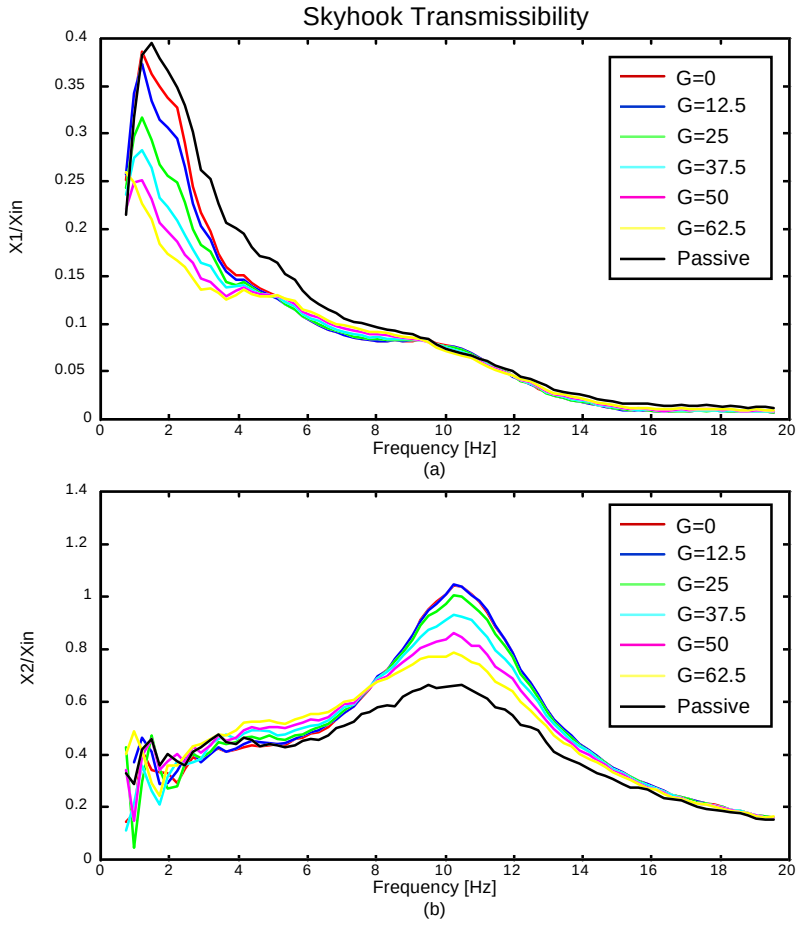

Figure 4.8. Suspension Transmissibility with Semiactive Skyhook Control
(a) Sprung Mass Transmissibility (b) Unsprung Mass Transmissibility

As the time traces in Fig. 4.9 show, the acceleration of the sprung mass with skyhook control is less than the acceleration of the sprung mass with a passive damper. More importantly, though, is the effect of increasing the skyhook gain. With increasing skyhook gain, the sprung mass acceleration is reduced, although the reduction at high skyhook gains can be accompanied by unacceptable unsprung mass motion.

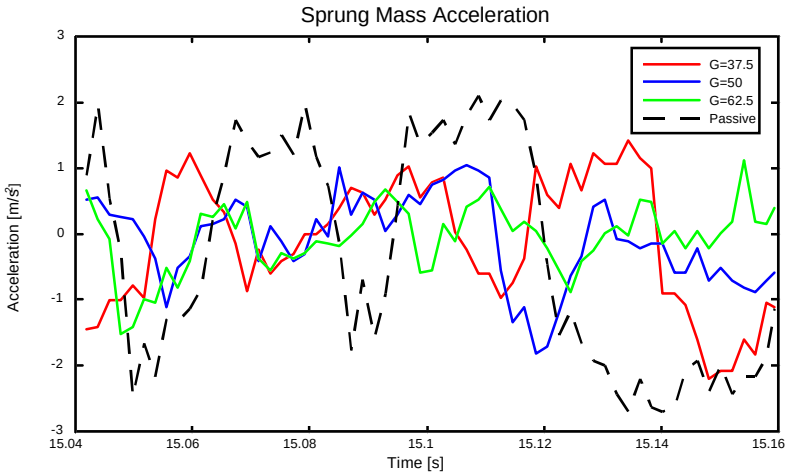

Figure 4.9. Sample Time Trace of Sprung Mass Acceleration with Skyhook Control

4.3.2 Groundhook Control

A time trace of the variables in the groundhook semiactive control algorithm is shown in Fig. 4.10. The groundhook control algorithm,

$$\begin{cases} -V_2 V_{12} > 0 & F_{SA} = C_{GND} V_2 \\ -V_2 V_{12} < 0 & F_{SA} = 0 \end{cases} \tag{4.5}$$

states that when the unsprung mass absolute velocity, V_2, and the relative velocity, V_{12}, have the same sign, the current to the MR damper should be zero. If V_2 and V_{12} have different signs, then the control signal should be on and proportional to V_2. The constant of proportionality in the Simulink implementation of the control is G, which is effectively C_{gnd} from Fig. 2.6.

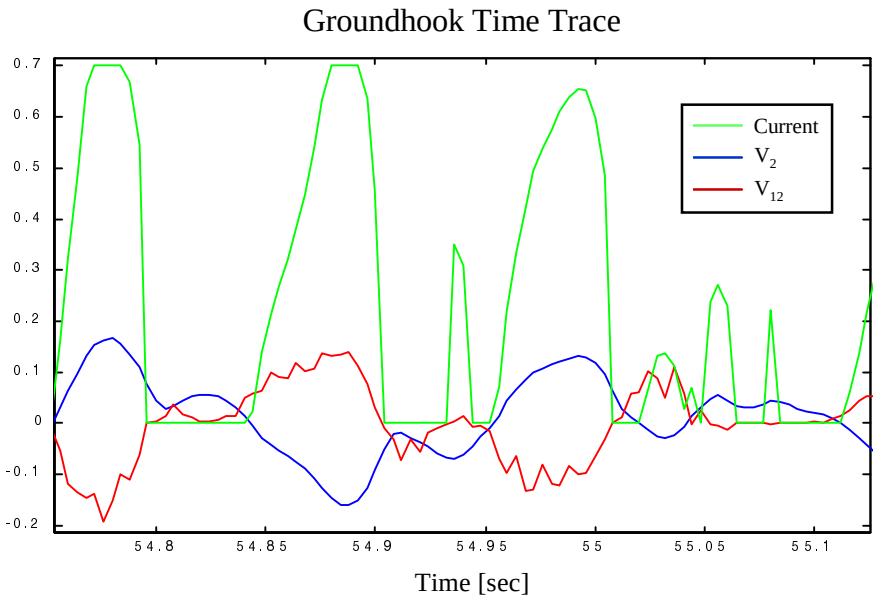

Figure 4.10. Sample Time History of Variables for Groundhook Control

As Fig. 4.10. illustrates, when V_2 and V_{12} have the same sign, the current to the damper is zero. When the signs are different, the control is on and proportional to V_2; however, any control signal greater than 0.7 is clipped. This clipping arises from the saturation block in the Simulink control block diagram and is present to prevent an over-current to the MR coil. Recall that the traced variables are reduced by one order of magnitude by Simulink, so the control signal is clipped at 7 Volts, which corresponds to the maximum allowable value of 1 Amp at the output of the current driver.

The transmissibility of the quarter-car under groundhook control is shown in Fig. 4.11. The attenuation of the unsprung mass natural frequency is evident with increasing groundhook control, as is the increase in the amplitude of the sprung mass resonant peak. As with skyhook control, high frequency isolation is improved with increasing groundhook gain, G.

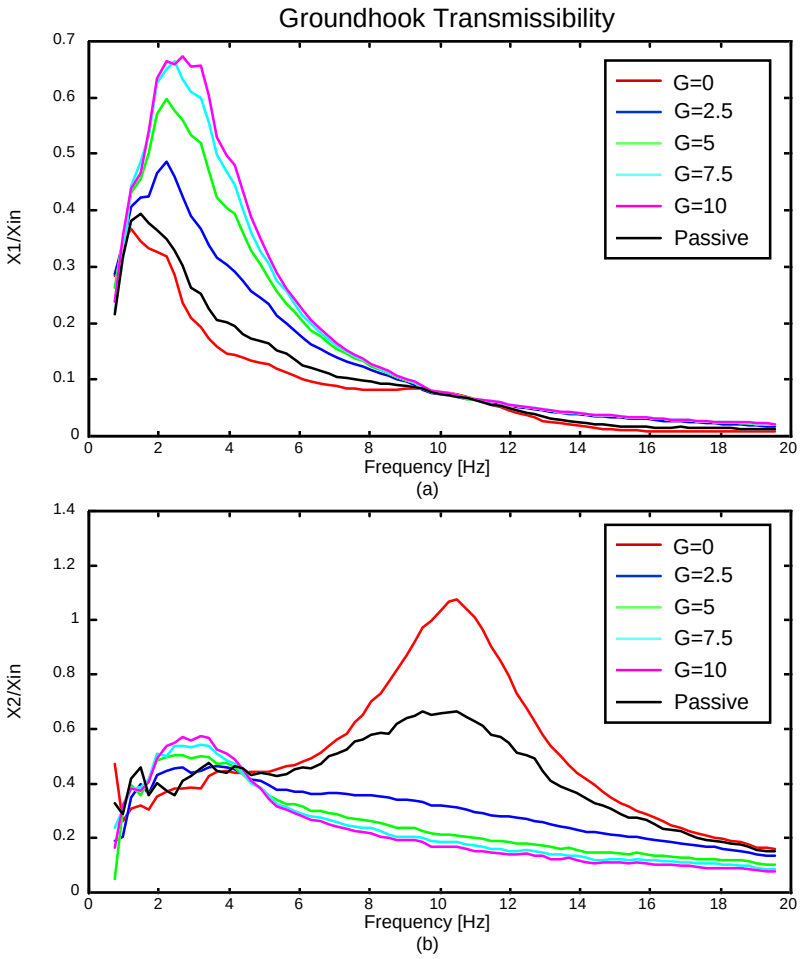

Figure 4.11. Suspension Transmissibility with Semiactive Groundhook Control
(a) Sprung Mass Transmissibility (b) Unsprung Mass Transmissibility

A time trace of the unsprung mass acceleration is shown in Fig. 4.12. The reduction in amplitude with increasing groundhook gain is evident; however, the reduction from passive damping is not apparent. At higher passive damping ratios, the effects on the unsprung mass acceleration are similar to the groundhook effect. When the two masses are coupled, as described in Section 4.2.2, there is a reduction in the unsprung mass motion due to the sprung mass being added to the unsprung mass, with the combined mass vibrating on the tire stiffness.

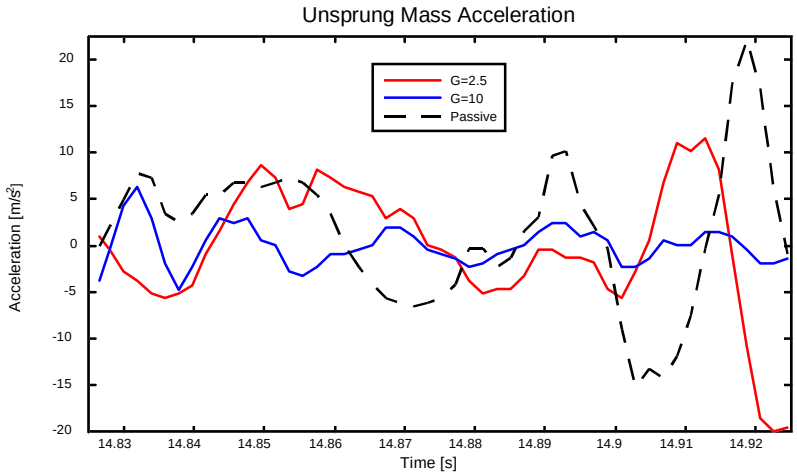

Figure 4.12. Sample Time Trace of Unsprung Mass Acceleration with Groundhook Control

4.3.3 Hybrid Control

As stated previously, hybrid control is a linear combination of skyhook and groundhook semiactive control, and can be written as

$$\begin{Bmatrix} V_1 V_{12} > 0 & \sigma_{SKY} = V_1 \\ V_1 V_{12} < 0 & \sigma_{SKY} = 0 \end{Bmatrix}$$

$$\left\{ F_{SA} = G\left[\alpha\sigma_{SKY} + (1-\alpha)\sigma_{GND}\right] \right. \tag{4.6}$$

$$\begin{Bmatrix} -V_2 V_{12} > 0 & \sigma_{GND} = V_2 \\ -V_2 V_{12} < 0 & \sigma_{GND} = 0 \end{Bmatrix}$$

implying that when α is 1, the control algorithm reduces to pure skyhook, and when α is 0, the control algorithm reduces to pure groundhook. As the transmissibility plots in Fig. 4.13 show, this effect is evident with the semiactive MR suspension. For a constant output gain G, as α nears 1, the sprung mass motion is attenuated at the expense of increased unsprung mass motion. Conversely, as α nears 0, the unsprung mass motion is attenuated at the expense of increased sprung mass motion. In fact, the responses of the system for α=1 and α=0 are identical to the skyhook and groundhook responses shown in Fig. 4.7 and Fig. 4.9. The second variable, G, then becomes the corresponding skyhook

or groundhook gain. The dynamic response of the system for different values of α is clearly a weighted combination of the skyhook and groundhook components of the semiactive hybrid control law. The effects of changing G, while keeping α constant, will be examined in the next section.

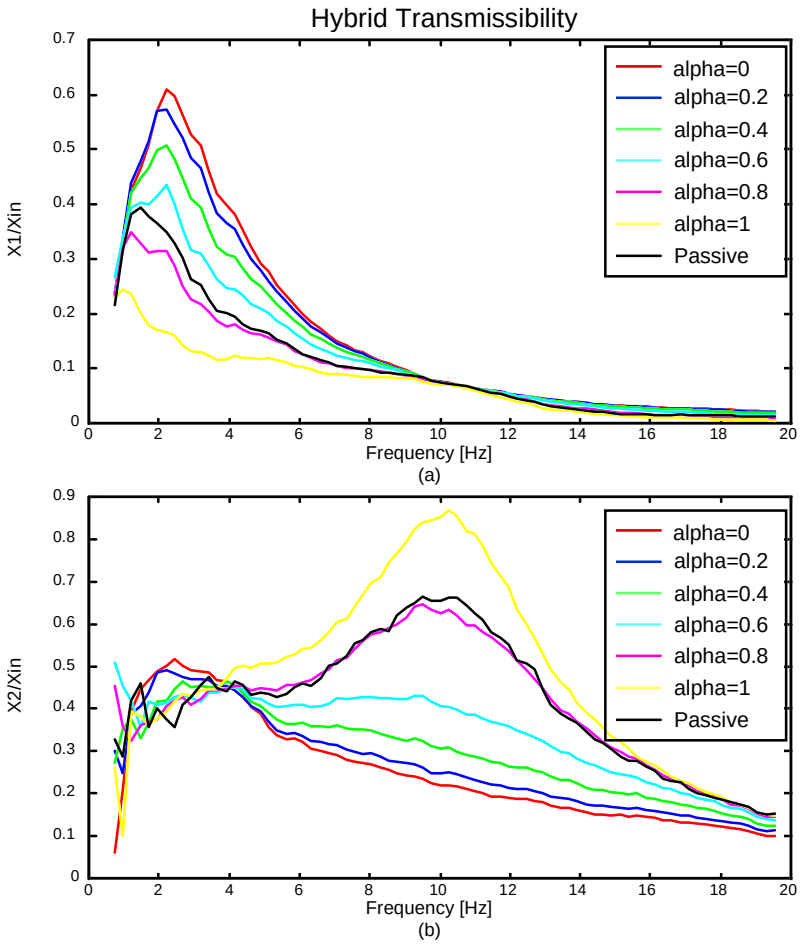

Figure 4.13. Suspension Transmissibility for Different Values of α (G=5)
(a) Sprung Mass Transmissibility (b) Unsprung Mass Transmissibility

The effect of changing α is also evident if one looks at the root-mean-square (RMS) sprung mass acceleration. The RMS sprung mass acceleration of a vehicle is a good indicator of passenger comfort. It quantifies the amount of acceleration being transmitted through the suspension and into the body of the vehicle, where the passengers

reside. For high values of α (i.e., approaching skyhook control), the RMS sprung mass acceleration is low. For lower values of α (i.e., approaching groundhook control), the RMS sprung mass acceleration is high. This high value indicates what we already know for groundhook control, namely, that it is good for controlling axle dynamics at the expense of sprung mass motion. The values of the RMS sprung mass acceleration for the different values of α are displayed in Table 4.1.

Table 4.1. RMS Sprung Mass Acceleration for Different Values of α

α	**RMS Sprung Mass Acceleration (m/s^2)**
0	1.576
0.2	1.525
0.4	1.429
0.6	1.299
0.8	1.110
1.0	0.942
Passive	1.1438

The transmissibility of the quarter-car for a low, fixed value of α is shown in Fig. 4.14. Since α is low, the controller weights the groundhook portion of the control more than the skyhook portion, and as such the response of the system resembles the response of a purely groundhook-controlled system.

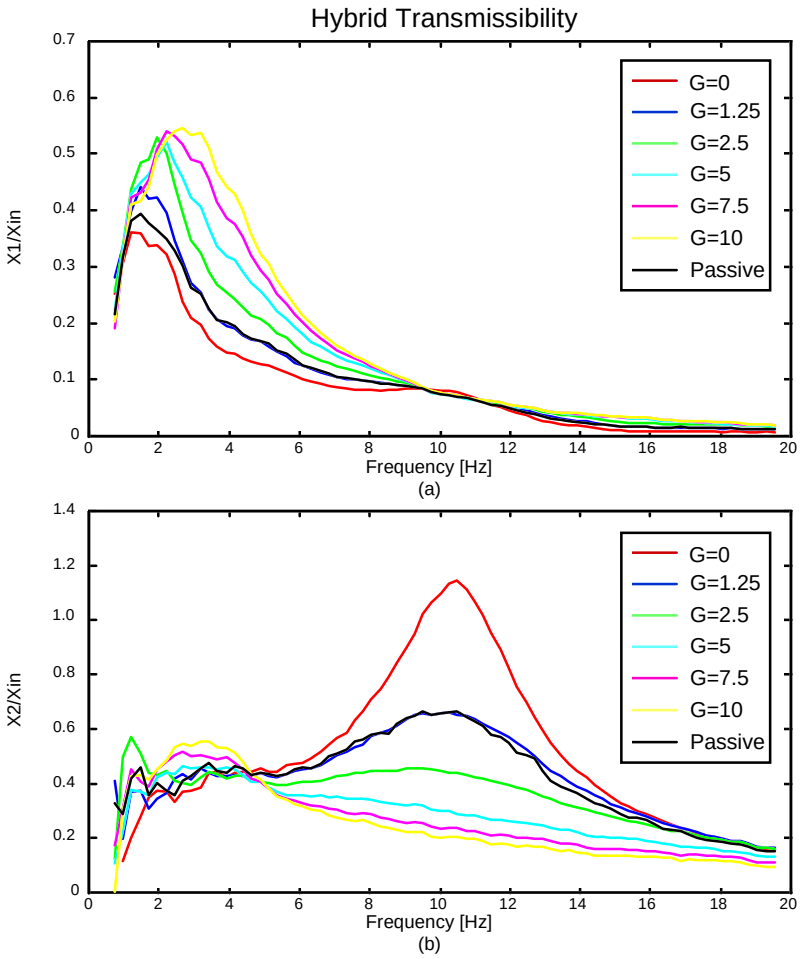

Figure 4.14. Suspension Transmissibility for Different Values of G (α=0.4)
(a) Sprung Mass Transmissibility (b) Unsprung Mass Transmissibility

4.4 Comparison Between Passive and Semiactive Dampers

If the transmissibilities for the three semiactive control cases and the passive case are plotted together, the relative benefits of semiactive control can be readily seen. As shown in Fig. 4.15, skyhook control sets the lower limit on the envelope of sprung mass motion, while groundhook control sets the upper limit. The opposite is true if we look at the unsprung mass motion: groundhook control sets the lower limit, while skyhook control and hybrid control with a high α set the upper limit.

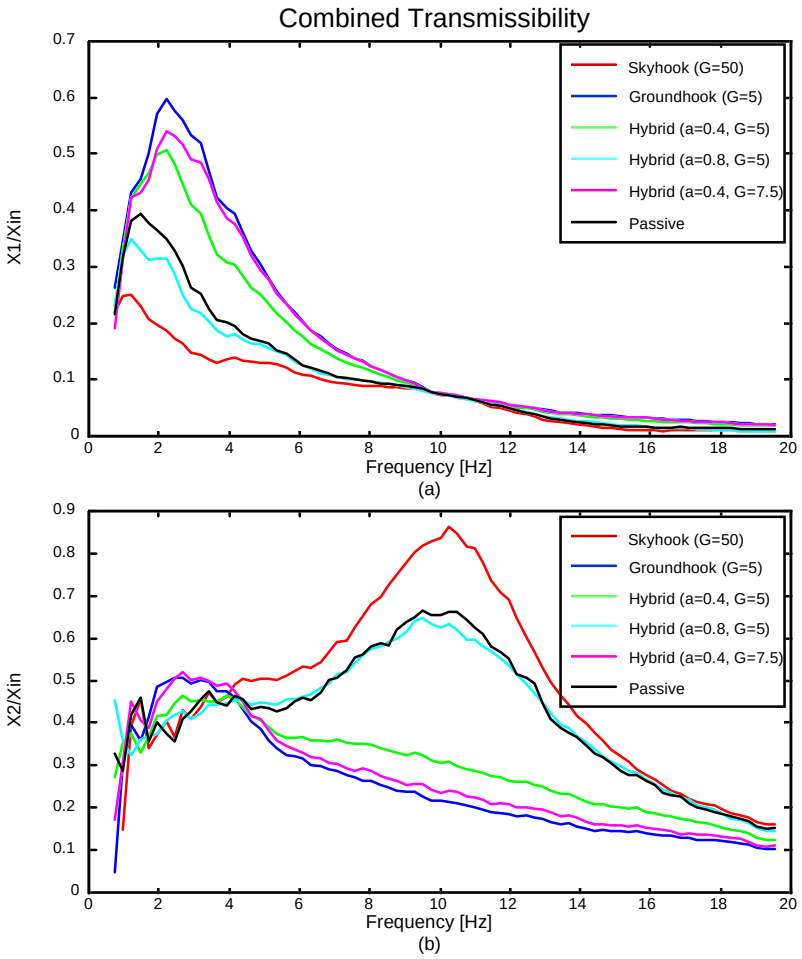

Figure 4.15. Transmissibility of Quarter-Car with Passive and Semiactive Damper
(a) Sprung Mass Transmissibility (b) Unsprung Mass Transmissibility

A time trace of the sprung mass acceleration reveals exactly what is happening to the sprung mass for the different semiactive and passive scenarios. As shown in Fig. 4.16, skyhook control and hybrid control with a high α greatly reduce the level of sprung mass acceleration, while groundhook control and hybrid control with a low α permit higher levels of sprung mass acceleration.

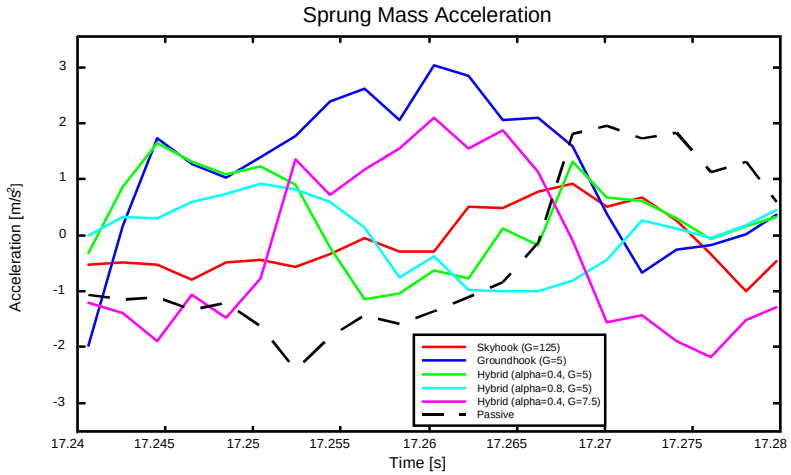

Figure 4.16. Sample Time Trace of Sprung Mass Acceleration with Passive and Semiactive Damper

Chapter 5

In-Vehicle Implementation

This chapter discusses the issues associated with implementing controllable dampers on a full size vehicle. The vehicle used for this study is a 1997 Chevrolet Lumina. First, the design issues associated with installing a damper that has a different geometry and configuration than the stock damper are discussed. Next, the methods for physically implementing the suspension control schemes are discussed. Finally, the actual system that will be installed in the vehicle is presented.

5.1 Retrofit of MR Dampers into Chevrolet Lumina

The vehicle used in this study is a 1997 Chevrolet Lumina 4-door passenger sedan. This vehicle belongs to the Hybrid Electric Vehicle Team of Virginia Tech (HEVT). The Lumina is a competition vehicle that is entered each year into the FutureCar Challenge, a national collegiate competition sponsored by the Department of Energy and the United States Council for Automotive Research (USCAR). The FutureCar Challenge is aimed at showcasing automotive technologies of the future. As such, the Virginia Tech FutureCar, shown in Fig. 5.1, was chosen as the vehicle on which to implement the magneto-rheological semiactive suspension system described in this work.

The stock Lumina suspension system utilizes a MacPherson strut damper configuration. A schematic of a MacPherson strut arrangement is shown in Fig. 5.2. MacPherson struts are frequently used in front-wheel-drive (FWD) vehicles due to space considerations. In a FWD vehicle, the transversely mounted engine and transaxle occupy much of the limited under-hood space. For this reason, it is not possible to use a double wishbone or short-long arm (SLA) suspension system, as the upper A-arm would have to occupy the same space as the transaxle/halfshaft system. Thus, front-wheel-drive

vehicles require the use of a suspension system with no upper A-arm and an outboard damper location, such as a MacPherson strut configuration.

Figure 5.1. The 1998 Virginia Tech FutureCar

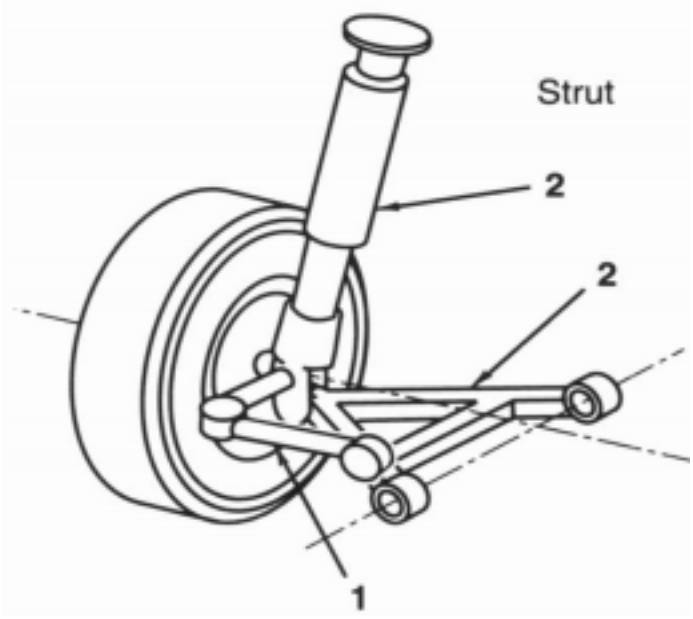

Figure 5.2. MacPherson Strut Suspension Geometry [26]

The MacPherson strut geometry, while beneficial from space considerations, requires a special type of damper. In a typical double A-arm configuration, the damper is a two-force member, exposed only to tension and compression forces. In the MacPherson strut configuration, the damper is a stressed member which must be able to sustain the bending moments applied to the damper during braking, accelerating, and cornering. For this reason, the damper rod on a strut is considerably larger in diameter than the rod on a straight push/pull damper. Figure 5.3 shows a side-by-side comparison of a strut-type damper and a conventional damper. Notice the much larger rod diameter on the strut-type damper.

(a) (b)

Figure 5.3. Comparison of Strut-Type and Push/Pull Only Dampers
(a) Strut-Type (b) Push/Pull Only

To accommodate the increased rod diameter, most strut-type dampers are twin tube dampers. A schematic of a twin tube damper and a monotube damper is shown in Fig. 5.4. Since more fluid is displaced with a larger rod diameter, the volume needed for the fluid to expand into is greater than the volume required in a monotube damper with a smaller rod diameter. Recall from Chapter 2 that a monotube damper typically utilizes a floating piston to accommodate the fluid volume displaced by the rod being inserted into the damper. The twin tube damper utilizes a foot valve which controls the flow of fluid into the outer tube. The foot valve is basically a check valve that greatly restricts the flow of fluid out of the inner tube (to force it instead through the orifice in the damper piston), but allows the easy flow of fluid from the outer tube to the inner tube to replace the volume created when the rod is extended out of the damper.

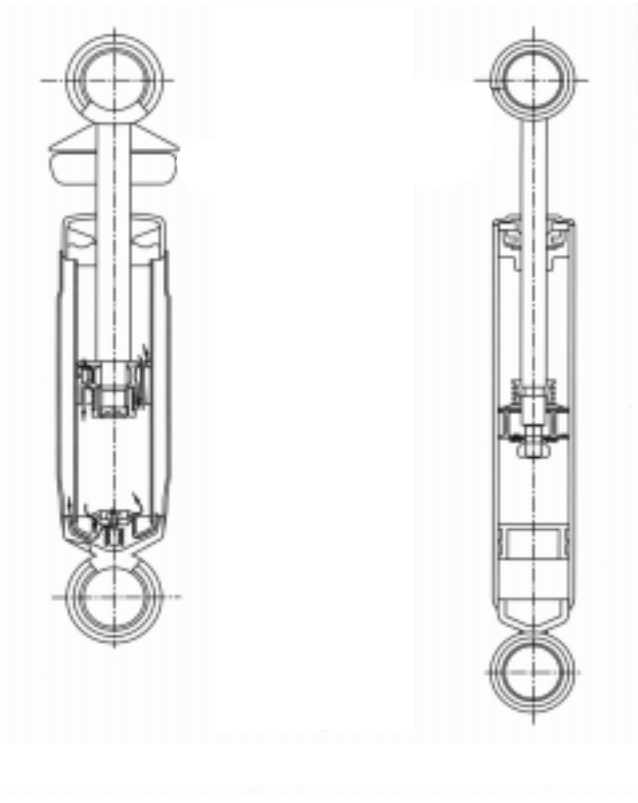

(a) (b)

Figure 5.4. Twin Tube and Monotube Damper Configurations
(a) Twin Tube (b) Monotube with Floating Divider [26]

The volume of the outer tube of a twin tube is far greater than the displaced volume that is attainable with the floating piston of a monotube. Thus, most strut-type dampers, including the stock dampers on the Lumina, utilize twin tube designs. However, due to the design constraints imposed by MR dampers, it was necessary to design and build monotube MR dampers for this research. With their relatively small rod diameters, the Lord/Koni MR dampers could not be installed on the Lumina in the same manner as the stock dampers or the rods would quickly yield under the bending moment applied during accelerating, braking, and handling maneuvers. An alternative mounting method needed to be devised for the MR dampers to work in the Lumina.

The alternative mounting method used consists of inverting the dampers (i.e., flipping the damper over so that the rod is on the bottom and the damper body is on the top). In this manner, the damper can be installed on the vehicle in such a way that the damper body is the load-bearing member and the damper rod experiences no bending moment. A schematic of the configuration is shown in Fig. 5.5. In this configuration, the damper rod is rigidly fixed to the strut housing on the unsprung mass of the vehicle. The damper body is then rigidly fixed above to the sprung mass (body) of the vehicle.

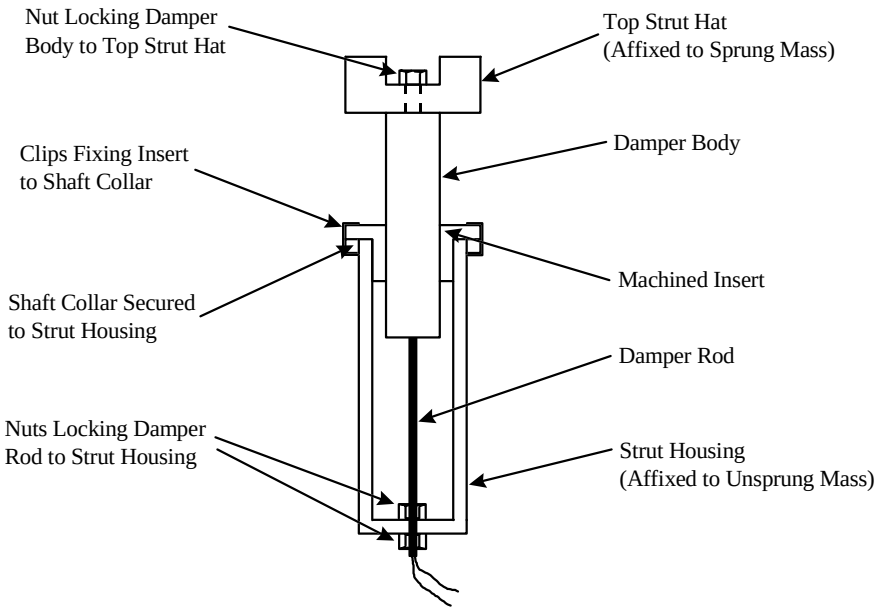

Figure 5.5. Schematic of MR Damper Installation

A critical component of this design is a Delrin slide bushing that can accommodate the relative motion between the damper body and the strut housing without allowing any lateral movement of the damper body. An insert was designed to precisely fit inside the top of the strut housing, following the stepped profile of the inside diameter of the strut housing. A bore was cut through the center of the insert with the same dimension as the outer diameter of the damper body. As shown in Fig. 5.5, the insert was affixed to a shaft collar that was then clamped to the outside of the strut housing. The physical system installed on the vehicle is shown in Fig. 5.6.

Figure 5.6. Physical Installation of MR Damper

5.2 Control System Used for In-Vehicle Testing

As stated in Chapter 3, in-vehicle implementation of skyhook, groundhook, or hybrid control would be identical to the quarter-car experimental setup used for this research. However, the sensors required for in-vehicle implementation of the above control policies are considerably more complex than the sensors used on the quarter-car apparatus. Not only do the sensors need to be small, rugged, and hermetically sealed from the under-car environment, but at least eight of them are required to outfit the four corners of a vehicle. Due to the time and cost constraints of this project, actual semiactive control of the suspension on the vehicle was not pursued. Rather, a lower cost means of utilizing the MR dampers for performance advantages has been developed.

The MR dampers actually installed on the Virginia Tech FutureCar are operated in a controllable passive state. In other words, the damping level desired is user-selected from the driver seat with two knobs mounted in the dashboard. One knob controls the current going to the front dampers, and the other knob controls the current going to the rear dampers. A schematic of the circuit designed for the dashboard-mounted knobs is shown in Fig. 5.7. The actual user interface in the dashboard is shown in Fig. 5.8.

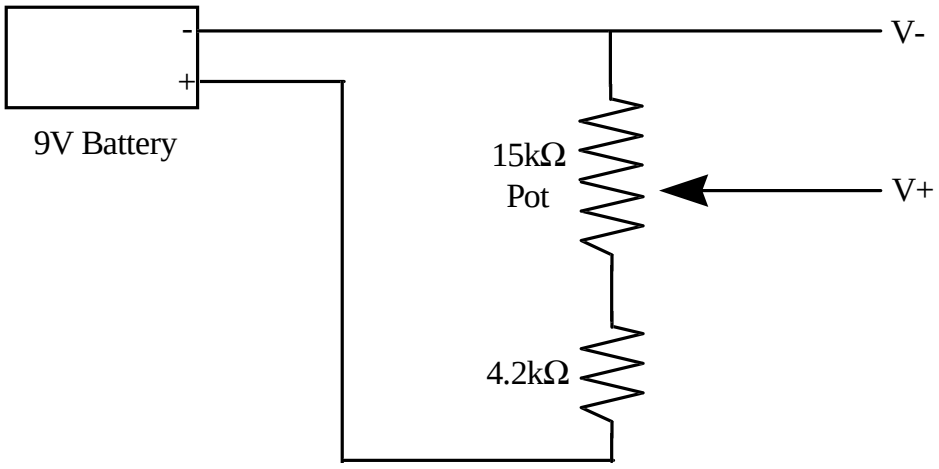

Figure 5.7. Circuit for User-Controllable Passive MR Suspension

Figure 5.8. Dashboard User Interface

The output of this circuit, V- and V+, interfaces with the input to the current driver shown in Fig. 3.22. The circuit is basically a voltage divider that drops the 9 Volts from the battery to approximately 7 Volts across the potentiometer. At 7 Volts, the current driver sinks 1 Amp through the MR damper, and since this is the most current that should be pushed through the MR damper, it is necessary to limit the full-scale input voltage to 7 Volts. As shown in the system schematic in Fig. 5.9, two such circuits are installed in the vehicle, with the V- and V+ output from the first circuit going to the current driver for the front dampers, and the V- and V+ output from the second circuit going to the current driver for the rear dampers.

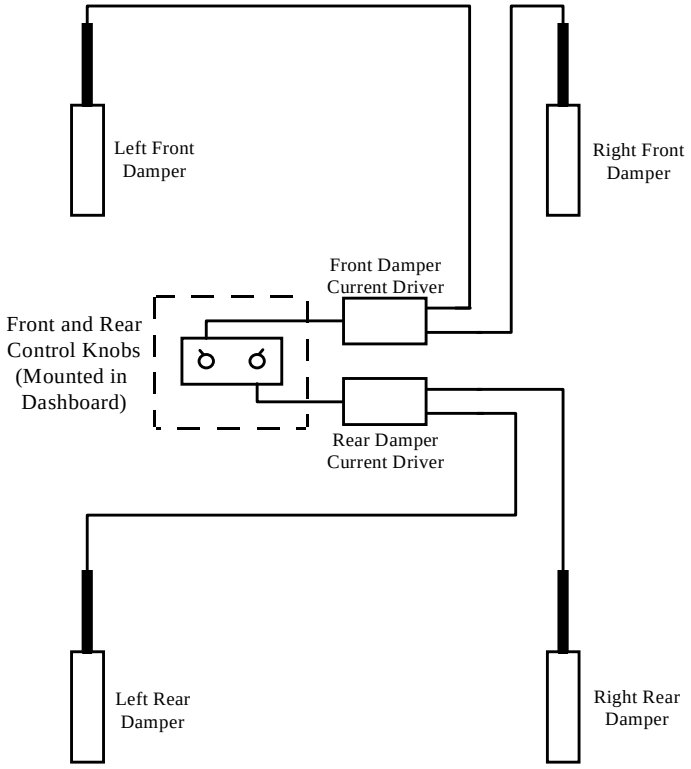

Figure 5.9. Schematic of System for Vehicle Installation

With independent front and rear damping adjustment, the user can quickly alter the oversteer/understeer characteristics of the vehicle on the fly. Increasing the rear damping level will increase the dynamic roll stiffness of the rear of the vehicle. The lateral load transfer due to the centripetal acceleration of the vehicle in a corner is divided between the front and rear of the vehicle based on the front and rear roll stiffnesses. With increased rear roll stiffness comes increased rear load transfer, yielding a higher vertical load on the outside rear wheel. This increased vertical load on the outside rear tire will force the rear tire to operate at a higher slip angle than the front tire, inducing oversteer. In addition, the converse is true: increasing the damping level of the front dampers will induce understeer because the front tires will be operating at a higher slip angle.

Chapter 6

Conclusions

The purpose of this chapter is to summarize the work that has been completed for this thesis. In addition, the results of testing will be discussed with respect to the research objectives set forth in Chapter 1. The chapter will conclude with several suggestions for future work that should be pursued in this area of research.

6.1 Summary

The objective of this research was to experimentally determine the dynamic response of a quarter-car for various semiactive control policies and compare the results to analytical predictions. In order to reach this objective, much preparatory work was completed. A full-scale quarter-car test apparatus was designed and built so that the single suspension system could be excited with any desired input and the output could be measured with a data acquisition system. A magneto-rheological damper capable of operating in a full-size vehicle was designed over the course of several months. Several meetings and phone conferences were held with sponsors Lord Corporation and Koni Incorporated to work out the details of a design that could be used in the Chevrolet Lumina test vehicle. Once the MR dampers were designed and in the process of being manufactured, the quarter-car test apparatus was set up at the Advanced Vehicle Dynamics Lab at Virginia Tech. A dSPACE AutoBox rapid controller development system was used both for control of the MR dampers and data acquisition of the sensors on the quarter-car.

The results of the research agree with the theoretical predictions of the passive and semiactive suspension configurations. Skyhook control was shown to be effective at isolating the motion of the sprung mass from the base excitation. The downside of skyhook control is that it allows excessive unsprung mass motion which may not be

desirable in practice. Groundhook control was shown to be effective at controlling the unsprung mass motion, but from a passenger comfort standpoint, groundhook control allows what might be considered excessive sprung mass motion. A linear combination of skyhook and groundhook, known as hybrid semiactive control, takes advantage of the benefits of both skyhook and groundhook. A hybrid semiactive controller, with two independent variables for the designer to specify, can be tuned to precisely yield the type of response desired.

6.2 Recommendations for Future Research

A natural extension of this work is to implement the semiactive suspension systems described earlier on the Virginia Tech FutureCar in a real-time embedded control mode. The groundwork is set: the dampers are installed on the vehicle and are currently controlled by the driver through a knob panel mounted in the dashboard. With the appropriate sensors, namely four hermetically sealed linear potentiometers, the dSPACE AutoBox can be used to automatically control the dampers in real time to achieve optimal suspension performance. This step is also a logical extension of the quarter-car testing that was performed for the skyhook, groundhook, and hybrid semiactive control policies.

If the real-time semiactive system is implemented with a position sensor to derive V_{12}, it would seem logical to investigate and implement end stop algorithms for the dampers. The benefit of an end stop algorithm is to avoid the situation where the damper bottoms out. If the stroke position is known, then the controller will know when the damper is reaching its physical travel limits and can adjust the damping radically.

With a working MR suspension system in a road-going full-size vehicle equipped with a dSPACE AutoBox and a laptop PC, the opportunities are endless. Much more complicated baseline control algorithms should be explored. Adaptive algorithms that monitor how aggressive the driver is driving could be used to update the suspension characteristics for weekend driving versus weekday commuting. Other vehicle parameters could be monitored and used for feedback control. Parameters such as vehicle

lateral and longitudinal acceleration could be fed back to the controller and used to set the damping levels of the four dampers independently. At large, positive, longitudinal accelerations such as accelerating from a stop, the rear dampers could be made very stiff to counteract the suspension squatting effects of rearward load transfer. Clearly, the same concept could be used to counteract nose dive during large negative longitudinal accelerations (braking). A lateral acceleration sensor could sense when the vehicle is entering a corner and stiffen the outside dampers. In addition, a lateral accelerometer located near the vehicle CG, combined with a yaw rate sensor, could be used to optimize the oversteer/understeer characteristics for every corner and every driving style by adjusting the front and rear damping levels while cornering.

References

1. Acker, B., Darenburg, W., and Gall, H., "Active Suspension for Passenger Cars," *Proceedings of the 11th Annual IAVSD Symposium*, 1991.
2. Yi, K. and Hedrick, K., "Dynamic Tire Force Control by Semiactive Suspensions," *Journal of Dynamic Systems, Measurements, and Control, Vol. 115*, No. 3, pp. 465-474, September 1993.
3. Valasek, M., Novak, M., Sika, Z., and Vaculin, O., "Extended Groundhook - New Concept of Semiactive Control of Truck's Suspension," *Vehicle System Dynamics, Vol. 27*, No. 5-6, pp. 289-303, June 1997.
4. Ahmadian, M., "A Hybrid Semiactive Control for Secondary Suspension Applications," *Proceedings of the Sixth ASME Symposium on Advanced Automotive Technologies*, 1997 ASME International Congress and Exposition, November 1997.
5. Crolla, D.A., and Abdel-Hady, M.B.A., "Active Suspension Control: Performance Comparisons using Control Laws Applied to a Full-Vehicle Model," *Vehicle System Dynamics, 20*, 1991.
6. Lieh, J., "Semiactive Damping Control of Vibrations in Automobiles," *Journal of Vibration and Acoustics, Vol. 115*, No. 3, pp. 340-343, July 1993.
7. Margolis, D.L., "The Response of Active and Semiactive Suspensions to Realistic Feedback Signals," *Vehicle System Dynamics, Vol. 11*, No. 5-6, pp. 267-282, December 1982.
8. Margolis, D.L., "A Procedure for Comparing Passive, Active, and Semiactive Approaches to Vibration Isolation," *Journal of the Franklin Institute, Vol. 315*, No. 4, pp. 225-238, April 1983.
9. Hwang, S., Heo, S., Kim, H., and Lee, K., "Vehicle Dynamic Analysis and Evaluation of Continuously Controlled Semiactive Suspensions Using Hardware-in-the-loop Simulation," *Vehicle System Dynamics, Vol. 27*, No. 5-6, pp. 423-434, June 1997.
10. Miller, L.R., "Tuning Passive, Semiactive, and Fully Active Suspension Systems," *Proceedings of the 27th IEEE Conference on Decision and Control*, December 1988.
11. Bellizzi, S. and Bouc, R., "Adaptive Sub-Optimal Parametric Control for Non-Linear Stocastic Systems: Application to Semiactive Isolators," *Probabilistic Methods in Applied Physics*, 223-238, 1995.
12. Hrovat, D., Margolis, D.L., and Hubbard, M., "An Approach Toward the Optimal Semiactive Suspension," *Journal of Dynamic Systems, Measurement, and Control, Vol. 110*, No. 3, pp. 288-296, September 1988.
13. Lazareva, T.G. and Shitik, I.G., "Magnetic and Magnetorheological Properties of Flowable Compositions Based on Barium and Strontium Ferrites and Iron Oxides," *Proceedings of the Society for Optical Engineering, Vol. 3040*, pp. 185-189, March 1997.

14. Ashour, O., Kinder, D., Giurgiutiu, V., and Rogers, C., "Manufacturing and Characterization of Magnetorheological Fluids," *Proceedings of the Society for Optical Engineering, Vol. 3040,* pp. 174-184.

15. Ashour, O., Rogers, C.A., and Kordonsky, W. "Magnetorheological Fluids: Materials, Characterization, and Devices," *Journal of Intelligent Material Systems and Structures, Vol. 7,* March 1996, pp. 123-130.

16. Carlson, J.D.; Catanzarite, D.M.; and St. Clair, K.A., "Commercial Magnetorheological Fluid Devices," *International Journal of Modern Physics B, Vol. 10*, No. 23-24, pp. 2857-2865.

17. Kordonsky, W., "Elements and Devices Based on Magnetorheological Effect," *Journal of Intelligent Materials, Systems, and Structures, Vol. 4*, pp. 65-69, January 1996.

18. Bolter, R., and Janocha, H., "Design Rules for MR Fluid Actuators in Different Working Modes," *Proceedings of the Society for Optical Engineering, Vol. 3045*, pp. 148-159, March 1997.

19. Jolly, M.R., Carlson, J.D., and Munoz, B.C., "A Model of the Behavior of Magnetorheological Materials," *Smart Materials and Structures, Vol. 5,* No. 5, pp. 607-614, October 1996.

20. Lane, J.S., Ferri, A.A., and Heck, B.S., "Semiactive Friction Damping for Suspension Control: Experimental Verification," *Proceedings of the 12th Triennial World Congress of the International Federation of Automatic Control, Vol. 3*, App. I, pp. 65-68, July 1993.

21. Karnopp, D., "Active and Semiactive Vibration Isolation," *Journal of Vibrations and Acoustics, Vol. 117,* No. 3B, pp. 177-185, June 1995.

22. Cebon, D., Besinger, F.H., and Cole, D.J., "Control Strategies for Semiactive Lorry Suspensions," *Proceedings of the Institution of Mechanical Engineers, Part D, Vol. 219*, No. D2, pp. 161-178, 1996.

23. Satoh, M., Fukushima, N., Akatsu, Y., Fujimura, I., and Fukuyama, K., "An Active Suspension Employing an Electrohydraulic Pressure Control System," *Proceedings of the 29th IEEE Conference on Decision and Control*, December 1990.

24. Miller, L. R., "An Introduction to Semiactive Suspension Systems," *Lord Library of Technical Articles*, Document LL-1204, 1986.

25. Crosby, M. J., Karnopp, D., et al., "Vibration Control Using Semiactive Force Generators," *Transactions of the ASME,* Paper 73-DET-122, June 1973.

26. Milliken, W.F., and Milliken, D.L., *Race Car Vehicle Dynamics*, Society of Automotive Engineers, Warrendale, PA, 1995.

27. Sancai, Lu, "Standardized Road Exciting Spectrum and Vibration Analysis of Vehicles," *5th International Pacific Conference on Automotive Engineering,* 1989.

28. dSPACE digital signal processing and control engineering GmbH, *User's Manual*, Real-Time TRACE Module, 1996.

Vita

Christopher A. Paré was born on September 14, 1974 in Attleboro, Massachusetts. He grew up in nearby Norton, Massachusetts, where his parents still live today. Chris graduated in 1992 from Norton High School, and enrolled in the University of Massachusetts Dartmouth to pursue a degree in Mechanical Engineering. He gained valuable Cooperative Education experience with Texas Instruments, where he spent several semesters and summers with both the Integrated Manufacturing Technologies group and the Automotive Sensors and Controls group. In 1996, he earned his Bachelor's in Mechanical Engineering, graduating Summa Cum Laude. After graduating from UMass Dartmouth and marrying his wife, Sarah, he moved to Blacksburg, Virginia to pursue his Master's degree at Virginia Tech, emphasizing controls and vehicle dynamics. In May 1998, he earned his Master's and went on to work for Texas Instruments in the Automotive Sensors and Controls group in Attleboro, Massachusetts.